Annals of Glaciology

Article

Cite this article: Zhaka V, Bridges R, Riska K, Hagermann A, Cwirzen A (2023). Initial snow-ice formation on a laboratory scale. *Annals of Glaciology* 1–18. https://doi.org/10.1017/aog.2023.58

Received: 7 March 2023
Revised: 30 June 2023
Accepted: 8 July 2023

Keywords:
Ice thickness measurements; ice/atmosphere interactions; sea-ice growth and decay; snow physics; snow/ice surface processes

Corresponding author:
Vasiola Zhaka; Email: vasiola.zhaka@ltu.se, vzhaka@yahoo.com

cambridge.org/aog

Initial snow-ice formation on a laboratory scale

Vasiola Zhaka[1], Robert Bridges[2], Kaj Riska[3], Axel Hagermann[4] and Andrzej Cwirzen[1]

[1]Department of Civil, Environmental and Natural Resources Engineering, Luleå University of Technology, 97187 Luleå, Sweden; [2]TotalEnergies SE, Paris, France; [3]Formerly TOTAL SA, Paris, France and [4]Department of Computer Science, Electrical and Space Engineering, Luleå University of Technology, 97187 Luleå, Sweden

Abstract

Snow ice (SI) forms from freezing wet snow, known as slush, and contributes to the thickness of level and brash ice. However, the mechanism of snow-slush-snow ice transformation has not been extensively investigated to date, despite the difference in the freezing rate of slush in comparison with water is important for estimating the ice thickness. In this study, we examined the growth of initial congelation ice (CI) and snow ice (SI) in a fresh water tank exposed to outdoor weather conditions in Luleå, northern Sweden. The tank of size $1.8 \times 0.65 \times 1.2$ m in length, width and height was divided into two compartments to facilitate the simultaneous growth of CI and SI. A total of 12 experiments were conducted in the years 2021 and 2022. The transformation from slush to snow ice was achieved by submerging various amounts of snow in the compartments. It was observed that approximately 35% of the initial snow transformed into SI. Snow ice grew 4 mm°C$^{-0.5}$ d$^{-0.5}$ faster than congelation ice. The CI growth under SI was 1 mm°C$^{-0.5}$ d$^{-0.5}$ slower than the CI growth under CI. This study provides valuable insights for modelling snow-slush-snow ice transformation and designing future laboratory-scale experiments.

1. Introduction

The submergence of snow in water forms slush, which consists of ice crystals suspended in water. The physical, thermal and optical properties of slush such as density, porosity, heat capacity or surface albedo, depend on the characteristics of both snow and water from which the slush originates. When exposed to low air temperatures, slush freezes to snow ice (SI). In comparison to congelation ice (CI), which is columnar ice formed from freezing water, SI is characterised by its granular microstructure (Ashton, 1986).

The submersion of snow and its subsequent transformation into slush and SI contribute significantly to the annual thickness of level ice. This has been evidenced by studying the ratio of the SI to total ice thicknesses, in various types of ice formations, such as fast sea ice, drifting ice, lake ice and river ice (Fichefet and Maqueda, 1999; Leppäranta and Kosloff, 2000; Jeffries and others, 2001; Shirasawa and others, 2005, Granskog, and others, 2006; Wang and others, 2015; Ohata and others, 2016). The formation of SI varies annually and by location, depending mostly on the amount of snowfall in the different weather conditions (Ohata and others, 2016).

Under natural environmental conditions, the formation of slush is driven by three main mechanisms: submersion, flooding and melting. Submersion occurs when the snow falls directly into open water, typically during early winter. In this event, the growth of level ice begins with snow-ice formation (Toyota and others, 2020). The submersion mechanism is particularly significant in winter navigation channels, where the snowfall accumulates on brash ice and submerges in water (between brash ice pieces) after a ship passage (Zhaka and others, 2020, 2021, 2023).

In the second mechanism SI forms at the snow/ice interface. As winter progresses, the weight of the snow accumulated on the level ice may exceed the buoyancy capacity of ice. If cracks or other conduits for water are present, the water level can rise above the surface of the ice, where the water mixes with snow and forms slush which freezes to SI (Leppäranta, 1983; Saloranta, 2000; Shirasawa and others, 2005; Ashton, 2011; Cheng and others, 2014).

Thirdly, slush and SI form, particularly in the spring when the snow melts due to increased solar radiation or precipitation (Machguth and others, 2023) and the meltwater subsequently refreezes to SI known as superimposed ice (Nicolaus and others, 2003; Granskog and others, 2006). The SI formation due to melting has been observed to change the surface albedo and delay the melting of ice (Perovich and others, 1998).

Several studies have investigated the natural snow-ice formation from snow flooding and snow melting. Due to a limited understanding of the snow-slush transformation process and the challenge of accurately estimating the initial slush thickness, making accurate predictions about SI growth remains difficult (Saloranta, 2000; Ashton, 2011; Cheng and others, 2014). Interestingly, the first mechanism of SI formation, which involves snow submersion in open water, has not been thoroughly studied or documented to the authors' knowledge (Toyota and others, 2020). This could be because this process occurs within a narrow time window at the beginning of the winter. Nevertheless, gaining a better understanding of how the initial snow-ice layer (formed from snow submersion in open water) affect the subsequent

https://doi.org/10.1017/aog.2023.58 Published online by Cambridge University Press

water freezing is important for ice growth modelling. A detailed investigation of the first mechanism can enhance our current knowledge of the snow-slush-snow-ice transformation, including the initial heat exchange between snow and water and its impact on the initial slush thickness and porosity. Furthermore, the current knowledge regarding slush transformation with time and environmental conditions can be improved, including aspects such as slush compaction, slush melting and freezing rate of slush in comparison with the freezing rate of water. This knowledge is a prerequisite for modelling the SI formation and growth, encompassing the three mechanisms mentioned above.

In addition, the first mechanism also relates to the contribution of snow to the accumulation and growth of brash ice. The snow submersion in ship channels and harbours may affect the brash ice consolidation between vessel passages. If the amount of incoming snow is significant between vessel transits, the vessel passage will mix the water with snow and slush will form among the brash ice (Zhaka and others, 2021, 2023). The slush will occupy the voids between brash ice pieces, and in the macropores, SI will form instead of CI. For example, if slush-filled macropores freeze faster than water-filled macropores, more ice will be formed between vessel passages. As a result, the consolidation rate and thickness of the brash ice will depend on the macroporosity and the snow thickness accumulated on brash ice. Therefore, when considering the growth models of brash ice, it is important to account the contribution of snow-slush-snow ice transformation process. However, this matter has not been previously investigated or addressed in relevant models such as those developed by Ashton (1974), Sandkvist (1986), Riska and others (2014, 2019).

This study investigates the first mechanism of snow-slush-snow ice transformation and compares its relevance with the other transformation processes occurring in coastal or lake ice. We investigate the slush formation from submerging snow, and the snow-ice formation from freezing slush and assess the difference in SI and CI growth rates. Additionally, we analyse the effect that the initial snow-ice layer has on the subsequent freezing of water. Furthermore, we examine the differences in the surface albedo between thin SI and thin CI since ice surface albedo affects the penetration of solar radiation into the ice and water below and, as a result, impacts the ice formation and melting.

The methodology and measurements are presented in the following section, and the snow-slush-snow ice transformation mechanisms are detailed in Section 3. Section 4 outlines the results, followed by deeper data analysis and discussion in Sections 5 and 6.

2. Method

Two laboratory-scale experiments campaigns were conducted in Luleå, northern Sweden, in two consecutive winters: February 2021, and February to March 2022. The experiments were conducted in a steel tank filled with fresh water, and were located outdoors as winter air temperatures in Luleå are continuously below 0°C for several months. During the first campaign, four experiments were performed, each lasting 8 h. In the second year, eight experiments were conducted in the same tank and location, with each experiment lasting 30 h.

To measure ice growth from freezing water and from freezing slush simultaneously, under the same meteorological conditions, the tank was divided into two compartments. The tank's exposure to the outdoor environment provided realistic conditions as environmental parameters, such as air temperature, snowfall, wind, humidity, and incoming radiation could not be controlled. The main measurements before the experiments included the snow mass and density, while during the experiment temperatures and thicknesses were recorded.

Note that the term 'laboratory scale' here refers to the size of the experiment rather than the conditions of the experiment.

2.1 Experimental setup

The tank was insulated around the side and bottom walls using 10 cm thick Styrofoam. A vertical steel dividing plate separated it into two different compartments (denoted here as R1 and R2). Each compartment had a surface area of 0.585 m^2 and a water depth of 100 cm. Four thermocouples were mounted in each compartment to measure the air, ice and water temperatures during the experiments.

In both campaigns, before the first experiment, the tank was filled with water and placed outdoors to lose heat and reach the freezing point. Then fresh snow was submerged artificially in one compartment while the freezing of water was investigated in the adjacent compartment. No external flows were introduced in the water column except when water was partly added or removed before and after each experiment to maintain a constant water depth of 100 cm.

In the first campaign, 6.9, 4.0 and 2.5 kg of snow were added to the water, in experiments labelled C1T01, C1T02 and C1T03 respectively. In C1T04, CI formation was observed in both compartments. In the second campaign, the mass of snow submerged in water was 1.5, 3, 4.5 and 6 kg. An identical snow mass was tested twice (C2T01 to C2T08), but the snow was added to a different compartment each time, see Table 1.

Snow density was measured using a snow cutter of a volume of 0.25 L in several positions in the fresh snow on land. The fresh snow was collected from the top layer of snow and placed in plastic buckets to measure its mass. Subsequently, the snow was distributed in the water. It is recognised that this procedure of snow immersion may have affected the snow properties, such as snow density and porosity. It was observed that the snow maintained

Table 1. Overall experimental matrix, including the time when the experiments were performed (dd/mm/yy), ID, ice type, snow mass, average snow density measured and snowfall occurrence during the experiment submerging in the water or accumulating on ice

Date	ID	Ice type	m_s kg	ρ_s kg m^{-3}	Snowfall
02/02/21	C1-T01 R1	CI	–	–	Yes
	C1-T01 R2	SI	6.9	120	Yes
03/02/21	C1-T02 R1	SI	4.01	128	No
	C1-T02 R2	CI	–	–	No
04/02/21	C1-T03 R1	CI	–	–	No
	C1-T03 R2	SI	2.5	103	No
05/02/21	C1-T04 R1	CI	–	–	No
	C1-T04 R2	CI	–	–	No
01-02/02//22	C2-T01 R1	SI	3	181	Yes
	C2-T01 R2	CI	–	–	Yes
08-09/02/22	C2-T02 R1	SI	6	113	Yes
	C2-T02 R2	CI	–	–	Yes
10-11/02/22	C2-T03 R1	CI	–	–	No
	C2-T03 R2	SI	1.5	116	No
14-15/02/22	C2-T04 R1	CI	–	–	No
	C2-T04 R2	SI	4.5	131	No
16-17/02/22	C2-T05 R1	CI	–	–	Yes
	C2-T05 R2	SI	6	137	Yes
21-22/02/22	C2-T06 R1	SI	1.5	96	Yes
	C2-T06 R2	CI	–	–	Yes
25-26/02/22	C2-T07 R1	SI	4.5	128	No
	C2-T07 R2	CI	–	–	No
08-09/03/22	C2-T08 R1	CI	–	–	No
	C2-T08 R2	SI	3	132	No

https://doi.org/10.1017/aog.2023.58 Published online by Cambridge University Press

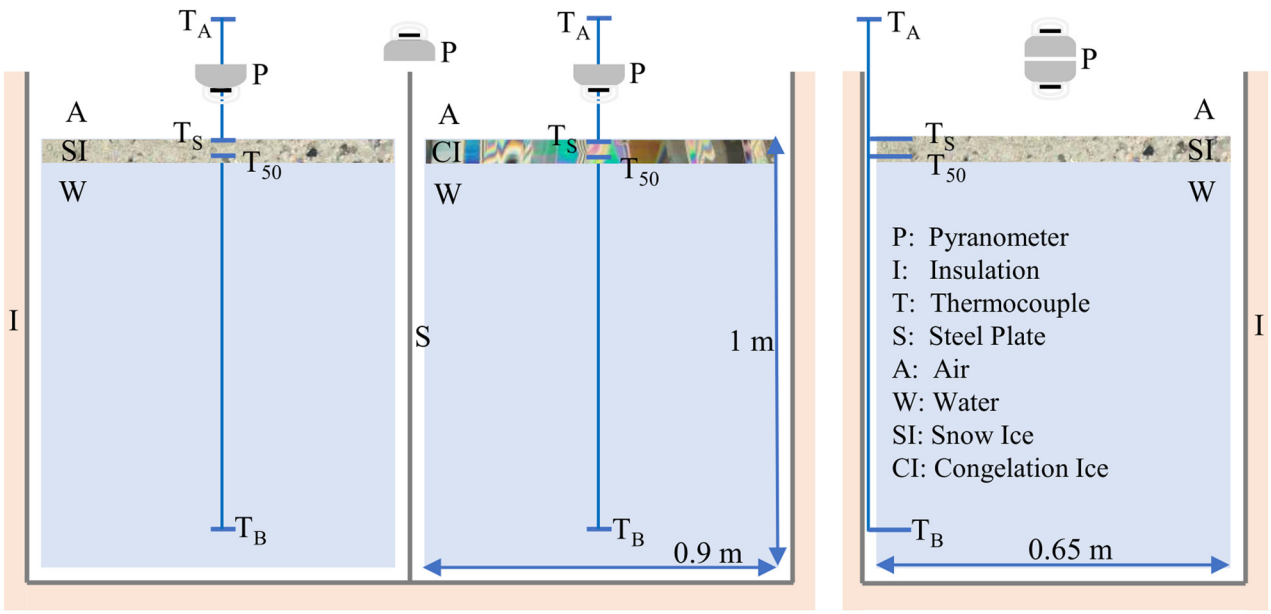

Figure 1. Tank set up with front (left) and side views (right). The tank is divided into a congelation (CI) and a snow ice (SI) section. The blue short vertical lines illustrate the position of each thermocouple. The position of the pyranometer when measuring the incoming radiation and the reflected radiation from the different surfaces is also illustrated. Not to scale.

its loose texture throughout the procedure, however, the grain size and shapes of snow crystals were not investigated.

Ice thicknesses in both compartments were manually measured four times during each experiment. In addition to the temperature and thickness measurements, incoming light was also recorded during the second campaign using a Hukseflux pyranometer SR30-M2-D1 (ISO 9060:1990 standard) with a sensitive spectral range of 285–3000 nm.

At the end of each experiment, the ice was mechanically broken and removed to empty the tank, which was then topped up with water the night before the next experiment. For the next experiment the surface was cleared once again by removing the ice formed during the night and the water level was corrected to the level of 100 cm. Figure 1 illustrates the experimental setup.

2.2 Temperature measurements

There are some differences in temperature measurements between the two experimental campaigns. In both campaigns, one thermocouple was placed 30 cm above the water level for air temperature measurements, and the second was mounted at the water's surface. In the first campaign, the third thermocouple was placed at a 30 mm depth and the fourth thermocouple was mounted at a depth of 80 mm, but in the second campaign the 3rd and 4th thermocouples were placed at depths of 50, and 900 mm, the last is assumed as the bottom of the tank.

In the first campaign (C1), the thermocouples were fixed along the wall of the tank and were angled to measure at a distance of 10 cm from the wall, but they were free-floating at the respective depths. Snow addition and possible water turbulences during the thickness measurements might have slightly displaced the thermocouples. In the second campaign (C2), the thermocouples were also fixed 10 cm from the wall, but with plastic plates attached to the side wall of the tank. As pointed out above, the ice formed in the tank was removed by mechanical breaking after each experiment. This process may have also displaced the vertical plates up to 15 mm below their initial positions.

The thermocouples were Type K wires connected to a TC-08 data logger and were monitored with PicoLog 6 software. Our thermocouples are classified as Tolerance Class 1, with an insulation rating between −75 and 260°C. The specified tolerance for class 1 thermocouples provided by the manufacturer is ±1.5°C. Details on sensor calibration are given in the supplementary material.

2.3 Thickness measurements

In the first campaign, the ice thickness in both compartments was measured every two hours, while in the second year, the thickness measurements was conducted after 6, 12, 24 and 30 h. The thickness measurements were conducted by drilling and sawing out several square ice pieces, each time at a different position. A schematic illustration of the sampling positions is given in Figure 2. The ice pieces were of different sizes for example up to 50 × 50 mm, see Figure 3. The thicknesses of the ice samples (SI & CI) were measured with a caliper. The slush underneath was merged with the SI, and it was possible to sample and measure its thickness. Lateral growth, up to 1 cm from the tank's walls was observed, however, the thickness measurements were carried out at least 10 cm from the walls.

In all the SI experiments of the first campaign and the first experiment of the second campaign, the initial slush thickness (HSL_0) which formed instantly after snow submergence was not measured. However, HSL_0 was calculated with an empirical regression equation that is detailed in Section 3. The construction of a small ruler with an angled protrusion at the end was suitable for measuring the initial slush thickness, in the seven following experiments. For this measurement, a small slush mass was carefully removed from the middle of the tank, and the ruler was used to determine the depth of the slush at the sides of the hole. Minor errors such as slush compression while measuring or not visually distinguishing the slush bottom when measuring may have occurred.

2.4 Radiation measurements

The pyranometer was placed between the two compartments, 20 cm above the water level, to continuously measure a representative

https://doi.org/10.1017/aog.2023.58 Published online by Cambridge University Press

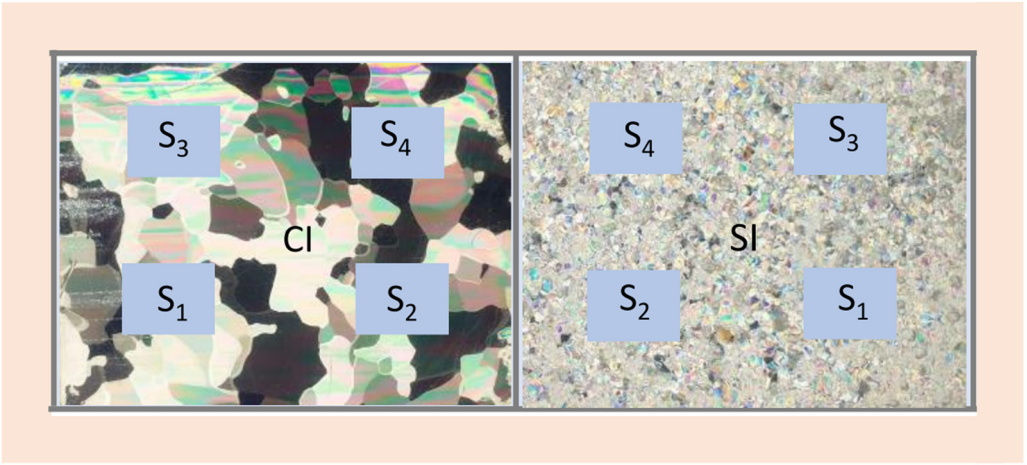

Figure 2. The top view of the tank experiments and the four ice sampling positions (S_1, S_2, S_3 and S_4) in each compartment. The congelation ice (CI) and snow ice (SI) surfaces are distinguished by their common microstructure. Not to scale.

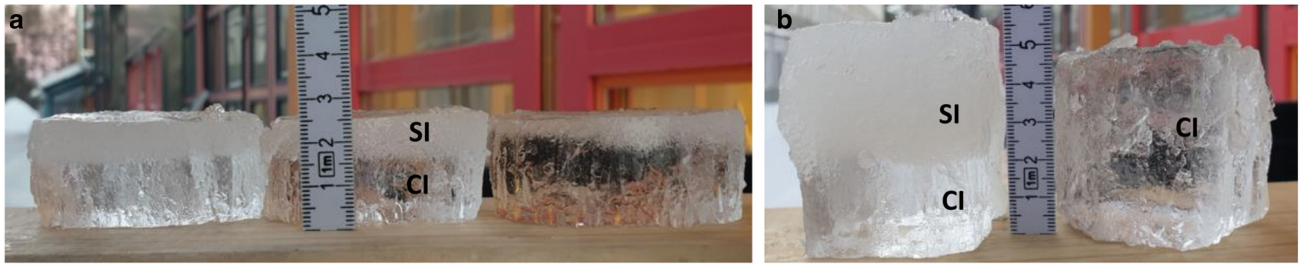

Figure 3. Examples of ice samples. (a) Three ice samples consisting of both congelation and snow ice; (b) the first sample consists of SI and CI underneath, while the second sample only of CI.

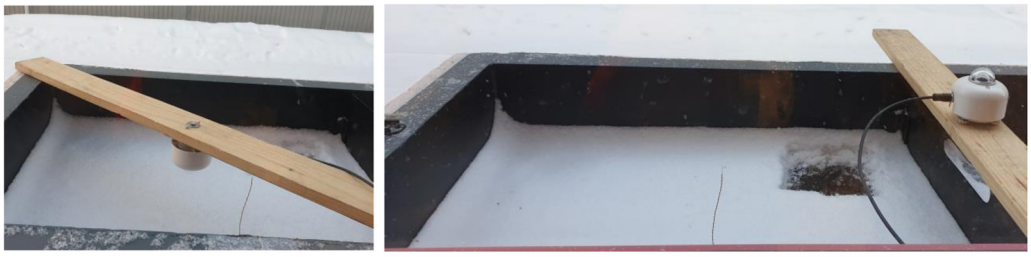

Figure 4. Top view of the second compartment during C2-T01 showing the pyranometer position when recording reflected radiation (left) and the pyrometer position between two compartments when recording the incident radiation (right).

value of the incoming solar radiation in both compartments, see Figure 4. The pyranometer was moved 3 to 5 times for a few minutes during the daylight to measure the outgoing radiation in both compartments 15 cm above the surface. Radiation measurements were calibrated considering the experimental setup. The detailed procedure for calibration is provided in the supplementary material. The albedo was calculated as the ratio between the measured incident and reflected radiation.

3. Results

In this section, the results obtained by the temperature and thickness measurements in both campaigns as well as the radiation measurements from the second campaign are summarised.

3.1 CI and SI thicknesses

This section provides an overview of the measured thicknesses of congelation ice (H_{CI}), snow ice (H_{SI}) and slush (H_{SL}) for all conducted experiments in both campaigns.

3.1.1 The first campaign (C1)

In the first three experiments, the slush layer was formed from the addition of 6.9, 4.0 and 2.5 kg of snow in T01R2, T02R1 and T03R2, respectively. During these experiments, only SI, and slush were present in the compartment where snow was submerged.

In T01, the CI and SI reached maximum thicknesses of 13 and 21 mm respectively, see Figure 5. The measured maximum thicknesses of CI and SI were 18 and 25 mm in T02 and 7.3- and 11.1-mm in T03. Referring to the total CI thickness, the H_{SI} was 61.5, 38.9 and 54.8% higher than H_{CI}, in T01, T02 and T03. During T01, snowfall occurred, and 5 mm of snow accumulated on the ice in both compartments. No snowfall occurred in the following experiments of C1.

The slush thickness decreased with time as the SI thickness increased. However, in T02 and T03, there was a deviation from this trend. For example, the measured slush thicknesses after 6 h were higher than those after 4 h. This suggests that the initial slush layer was uneven due to manual snow distribution at the beginning of the experiment.

https://doi.org/10.1017/aog.2023.58 Published online by Cambridge University Press

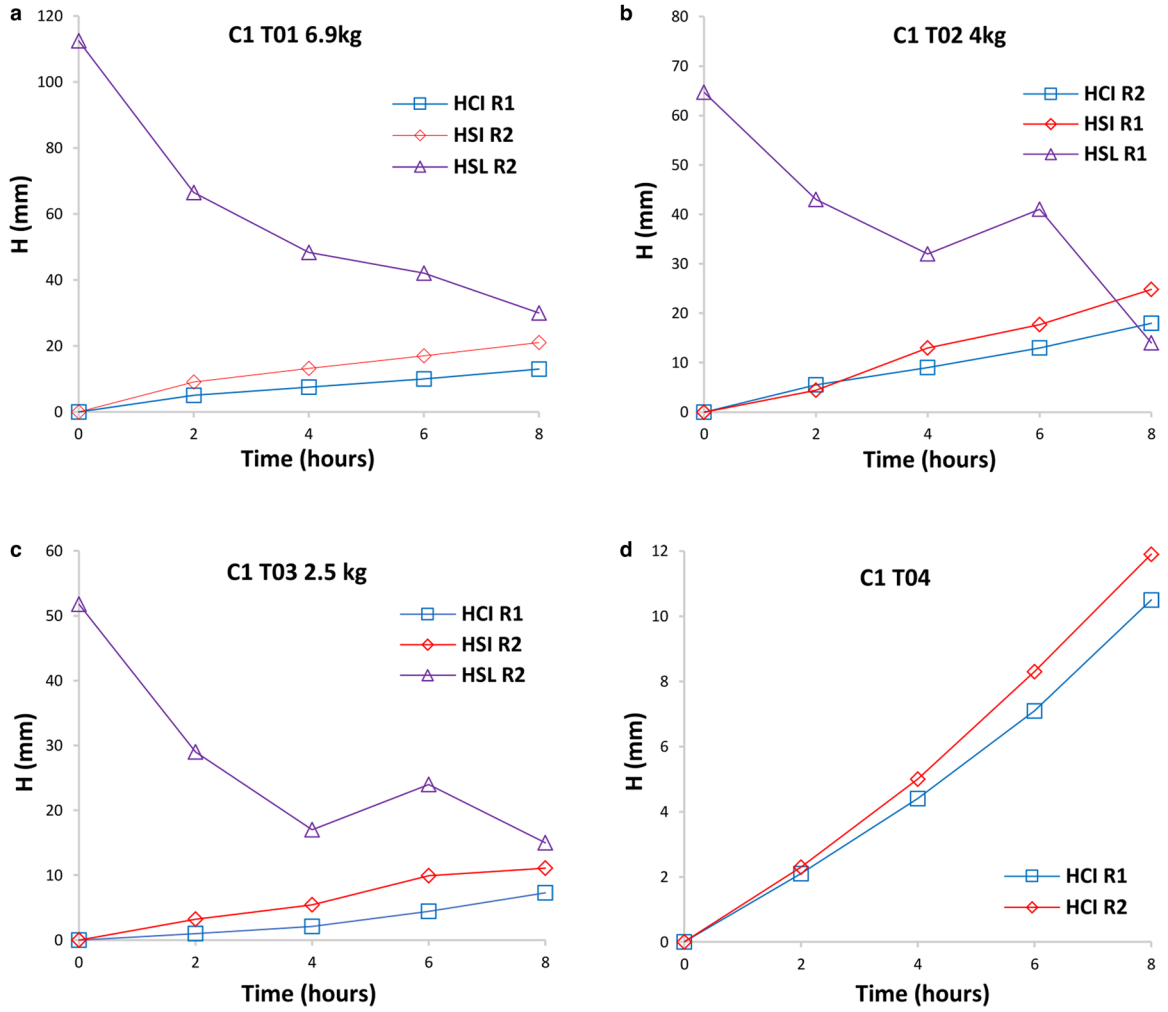

Figure 5. Measured thicknesses of congelation ice, snow ice and slush (HCI, HSI and HSL) in the first campaign (C1). Figures a, b, c and d illustrate the results from the first, second, third and fourth experiments (T01, T02, T03, and T04), respectively. Snow was added only in one compartment (R1 or R2) in each of the first three experiments.

In T04 the growth of CI was investigated in both compartments. The maximum thickness of CI in each compartment was 10.5 and 11.9 mm, respectively. The variation in CI growth between compartments is attributed to the experimental error that may occur. In the initial ice formation phase, thickness measurements are more sensitive and prone to experimental errors compared to the later stages of ice growth (Toyota and others, 2020).

3.1.2 Second campaign (C2)

In the second campaign, the slush layer was created by adding 1.5 kg of snow in T03, and T06; 3 kg of snow in T01 and T08; 4.5 kg of snow in T04 and T07; and finally, 6 kg of snow in T02 and T05. During these experiments, CI formed beneath the SI due to the longer experiment duration. The total thickness of the initial SI and the CI formed underneath is represented as H_T. The thickness results from C2 are given in Figs 6a–p.

In the first experiment (T01), the slush transformed into SI within 6 h. After 30 h the total ice thickness (H_T) was 8 mm thicker than CI. Snowfall occurred during the experiment, and the maximum thickness of snow accumulated on ice was 25 mm.

In T02, the initial slush layer had a thickness of 113 mm and formed a SI thickness equal to 36 mm. At the beginning of the experiment, a light snowfall occurred and contributed to slush formation in both compartments, but no dry snow accumulated on the ice. The total amount of incoming snow that was submerged in both compartments during the first 6 h was approximately 15 mm. This snowfall formed a 10 mm thick SI layer after 24 h, in the compartment where no snow was added. The ice thickness was 11 mm higher in the compartment where 6 kg was initially added.

In T03, an initial slush layer of 25 mm formed a SI thickness of 8 mm which remained unchanged after 12 h. H_T was 5 mm higher than H_{CI}. In T04, the 4.5 kg of snow submerged formed a 70 mm thick slush layer. This transformed to a 28 mm thick SI after 12 h. The difference in ice thickness between compartments was 7 mm, with maximum thicknesses of 63 and 56 mm, respectively.

In T05, 6 kg of snow formed a slush layer of 80 mm. Snow continued to fall throughout the experiment, leading to the formation of a SI layer in both compartments. After 30 h, a thick layer of dry snow (120 mm) accumulated on the ice. In the compartment where an initial snow mass was added, the slush layer did not freeze completely and SI reached a thickness of 19 mm, while the slush underneath was 8 mm thick. In the other compartment, the total ice thickness was 15 mm comprising both SI and CI.

In T06, 1.5 kg of snow formed a slush layer equal to 30 mm. The slush froze after 6 h and formed a 12 mm thick SI layer. The thickness difference between compartments was 4 mm. In T07, 4.5 kg of snow formed a slush layer equal to 75 mm which transformed completely to SI after 24 h. In T08, 3 kg of snow yielded a slush thickness of 40 mm, and the SI had a maximum thickness of 18 mm after 24 h.

https://doi.org/10.1017/aog.2023.58 Published online by Cambridge University Press

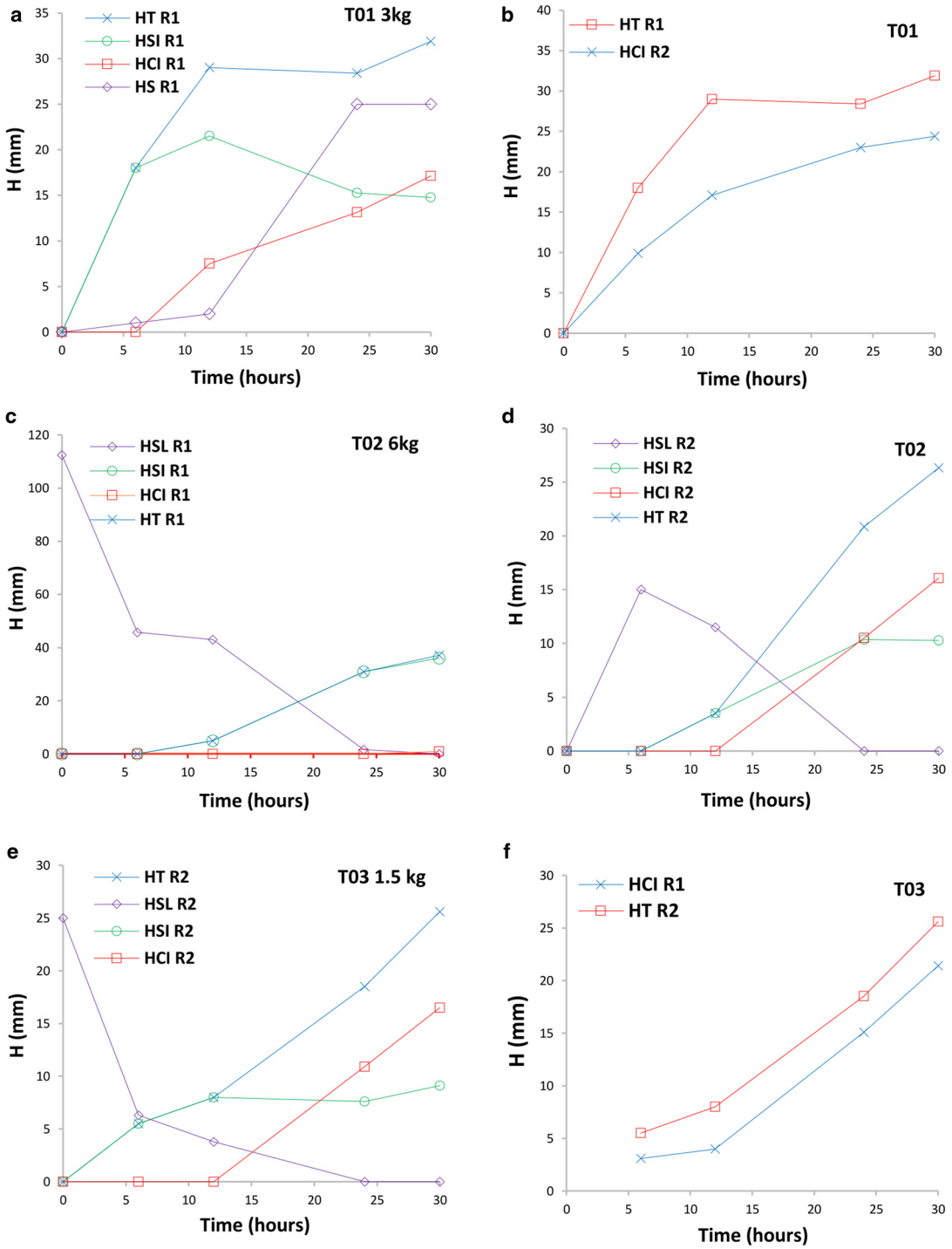

Figure 6. Measured thicknesses of congelation ice (HCI), snow ice (HSI), slush (HSL) and snow (HS) in both compartments (R1 and R2) for all the experiments (from T01 to T08) carried out in the second campaign (C2). HT is the sum of HSI and HCI in the compartments where the total solid ice is comprised of both ice types. The amount of snow added to one of the compartments in each experiment is given in the title of each plot.

After 24 and 30 h, the thicknesses of SI were 18 and 15 mm in T07R1 and 21 and 17 mm in T08R2. Even though the snow was distributed carefully in the water, the decrease of the SI thickness with time indicates an uneven initial slush layer. In addition to the mechanical distribution, the difference in the slush thickness and snow concentration was also a result of snow agglomeration when submerged into the water.

3.2 Temperature recordings

Examples from the continuous temperature recordings from both campaigns are given in Figs 7 and 8. During C1-T01-R1, the surface thermocouple initially measured the air temperature near the water surface, followed by the ice temperature see the red line in Figure 7. In C1-T01-R2, the temperature recordings on the surface and at depths of 30 and 80 mm remained above 0°C throughout the experiment and reached the similar values after approximately one hour. This indicates the displacement of the thermocouples beneath the slush layer or at the water/slush interface due to the snow addition. In the second compartment (R2), the surface thermocouple recorded a temperature peak some minutes after the start of the experiment, which indicated the cooling of water from snow submergence.

https://doi.org/10.1017/aog.2023.58 Published online by Cambridge University Press

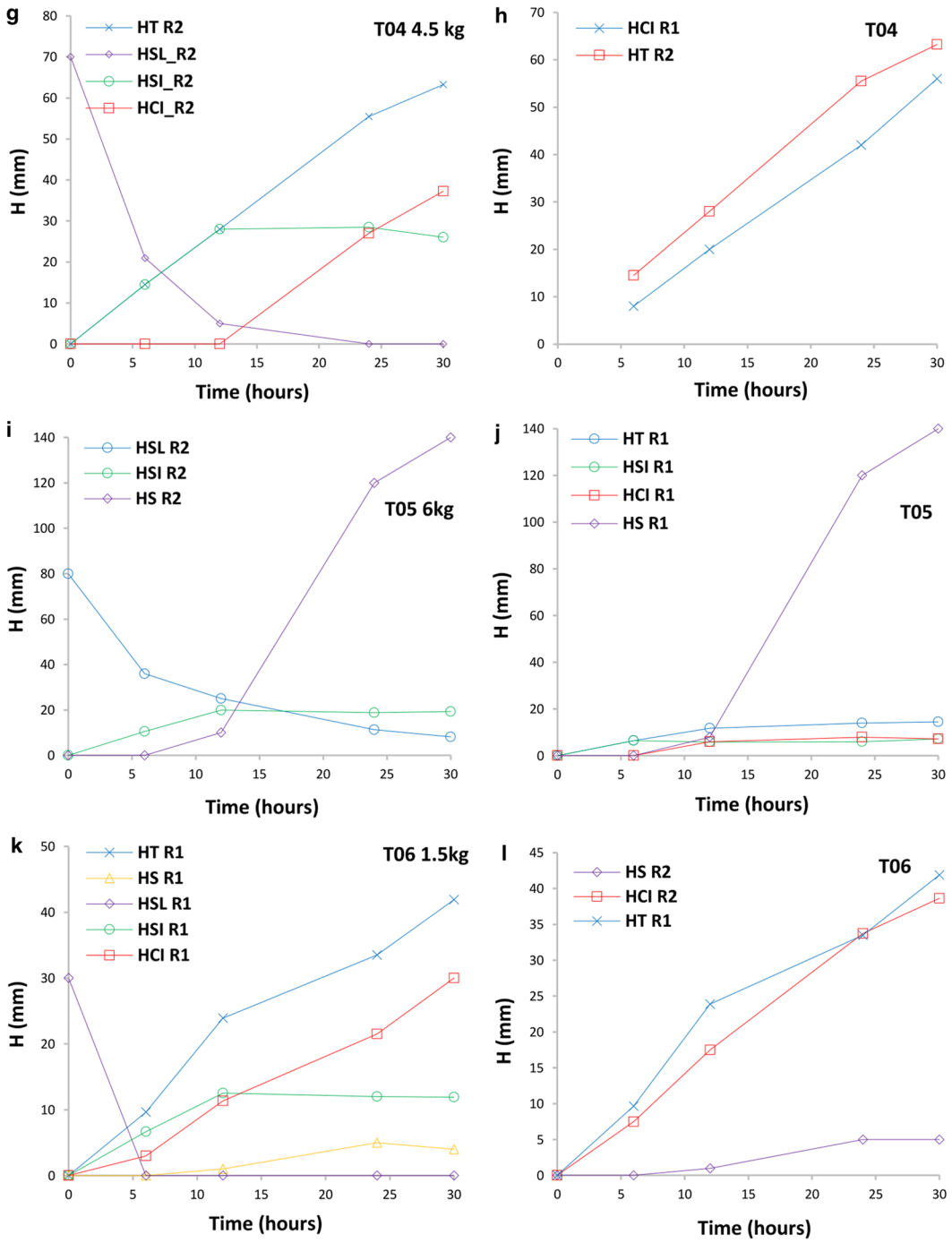

Figure 6. Continued.

In the second campaign, the thermocouples were fixed in plastic plates, ensuring that the snow submergence did not displace them. This is evidenced by the negative temperatures recorded by the surface thermocouples. In the first compartment where no snow was added, the water surface reached the freezing point after approximately four hours, see Figure 8. Contrary to C2-T05-R2 the water cooling occurred instantly due to snow addition in the water.

Thermocouples at 50 mm depth recorded negative temperatures in all C2 experiments, even when the total CI thickness was below 50 mm. A possible explanation for this occurrence can be the displacement and freezing of the thermocouple tip. Therefore, the temperature recordings cannot be accurately correlated with the original depth of thermocouples. However, the air temperature recordings and the temperature difference between thermocouples are considered reliable in the current analysis.

3.3 Shortwave radiation

The incoming solar radiation recorded in the tank was compared with data recorded by the SMHI meteorological station at Luleå airport. Two examples of incoming solar radiation during T01 and T08 are illustrated in Figure 9. In T01 the radiation difference between SMHI and the tank recording was about 90 W m^{-2}, while in T08 this difference reached up to 100 W m^{-2}. This variation can be attributed to the tank's location between two buildings, which shaded the tank and limited its exposure to direct sunlight. As a result, the tank primarily received diffuse solar radiation.

Figure 10 illustrates the reflected radiation from the ice surfaces in both compartments for T01 and T08. In T01, at the beginning of the experiment, the reflected radiation measured in the first compartment was higher compared to the second compartment. This difference can be attributed to different surfaces: R1 had a surface

https://doi.org/10.1017/aog.2023.58 Published online by Cambridge University Press

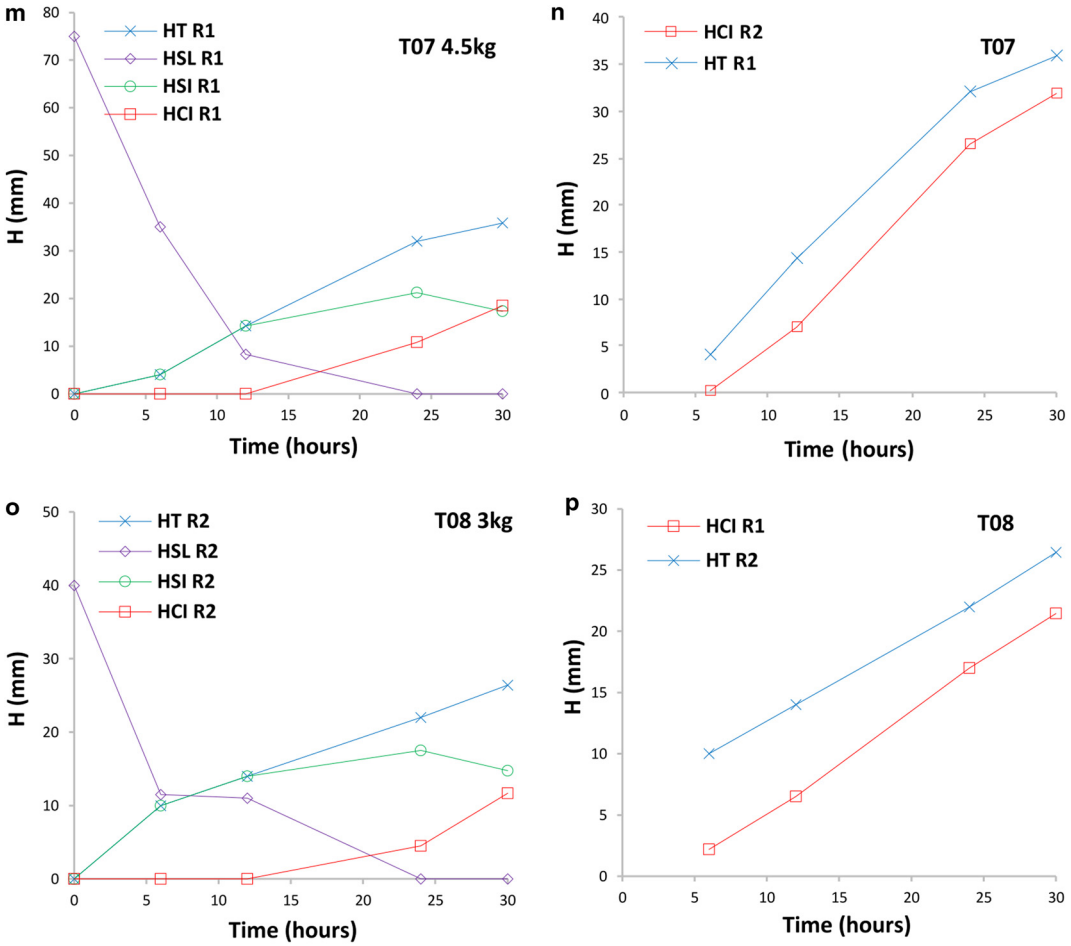

Figure 6. Continued.

consisting of slush, while R2 consisted of water. However, over time, snowfall accumulated on ice, and the reflected radiation resulted in almost similar values in both compartments. In T08, throughout the experiment, the reflected radiation from R2 was higher than that from R1. This difference was due to the SI formation in R1 while only CI was formed in R2.

Figure 11 illustrates the albedo calculated as the ratio of incident radiation to reflected radiation. An average albedo was calculated as the mean value of all measured daytime surface albedos (for incoming solar radiation higher than zero) during the 30 h of the experiments. This average value considers the albedo values from the beginning of the experiment when only slush or water

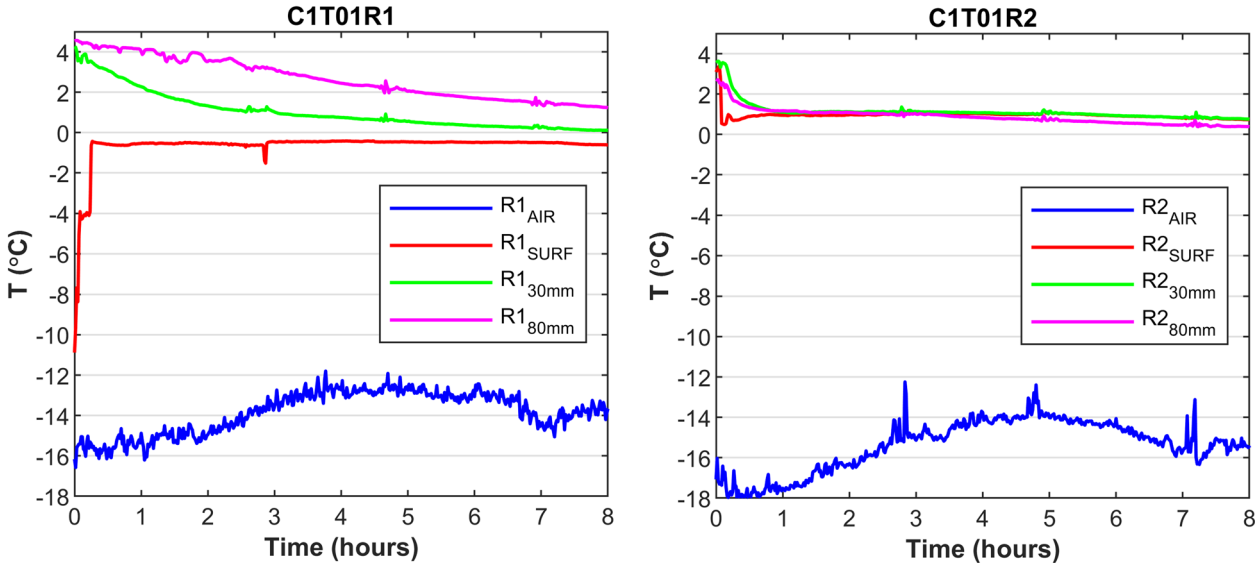

Figure 7. Continuous temperature readings during the first experiment of the first campaign. Congelation ice formation was investigated in the first compartment (R1), while in the second compartment (R2) 6.9 kg of snow was submerged in water. The blue, red, green and purple lines show the temperature recordings throughout the experiment, e.g., for the first compartment in the air ($R1_{AIR}$), at the surface ($R1_{SURF}$), at depths of 30 mm ($R1_{30mm}$) and 80 *mm* ($R1_{80mm}$).

https://doi.org/10.1017/aog.2023.58 Published online by Cambridge University Press

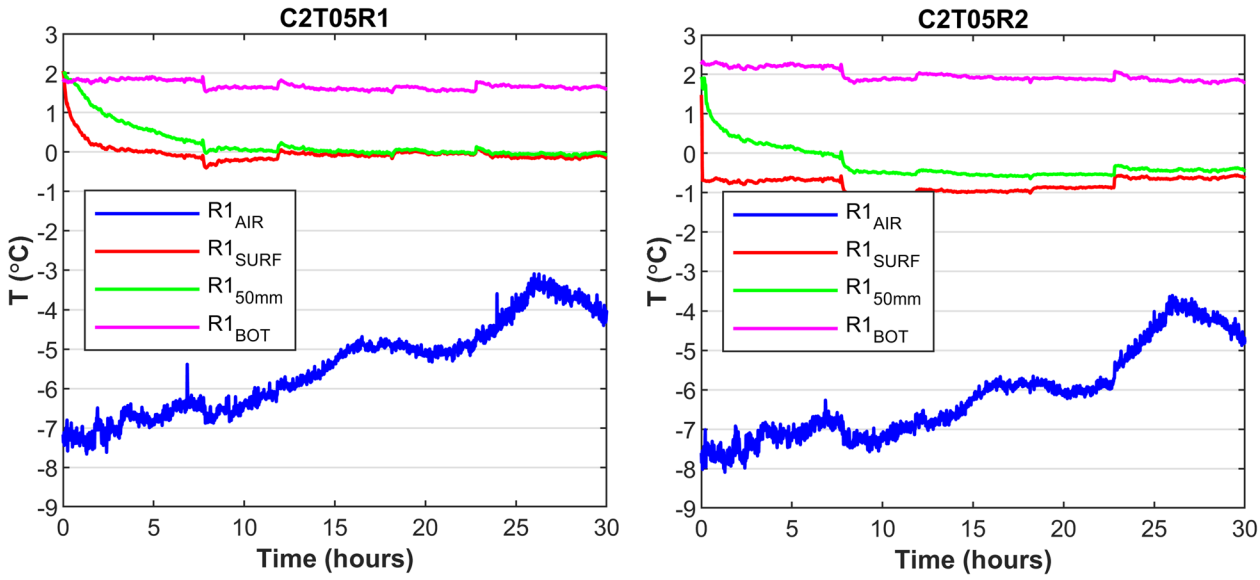

Figure 8. Continuous temperature readings during the fifth experiment of the second campaign. Congelation ice formation was investigated in the first compartment (R1), while in the second compartment (R2) 6 kg of snow was submerged in the water. The blue, red, green and purple lines show the temperature recordings throughout the experiment, e.g., for the first compartment in the air ($R1_{AIR}$), at the surface ($R1_{SURF}$) and depths of 50 mm ($R1_{50mm}$) and 900 mm ($R1_{BOT}$).

was present until the end of the experiment when the ice was covered with snow. The reflected radiation illustrated in the first plot of Figure 10 from the 23rd to 27th hour corresponds to an average albedo of 0.83 in both compartments. This value is representative of snow-covered surfaces (Grenfell and Maykut, 1977; Perovich, 1996; Perovich and others, 2002).

4. Snow-slush-snow ice transformation theory

This section outlines the theory, assumptions and model formulations pertaining to snow-slush-snow ice transformation, as used in this study.

4.1 Slush formation

Snow will completely submerge in water (unless it falls on ice and accumulates as dry snow). If the water surface temperature is uniform, and close to the freezing point, the natural snowfall into the water will form a slush layer. In this study, the snow was distributed by hand, so some horizontal variation of the slush thickness can be expected.

The initial slush thickness (H_{SL0}) is governed by the initial amount of snow that is distributed in the water. The theoretical uniform snow thickness H_s evenly distributed on a dry surface equal to the compartment's surface area ($A_R = 0.585\ m^2$) was estimated from the mass and density measurements as:

$$H_s = \frac{1}{A_R} \cdot \frac{m_s}{\rho_s}, \tag{1}$$

where m_s is the snow mass, and ρ_s is the snow density, see Table 1.

It is assumed that H_s is the initial snow thickness submerged in water and all the air pores of snow are replaced with water. The air/snow fraction is then assumed to be equal to the water/ice fraction (Adolphs, 1998), and the initial slush thickness (H_{SL0}) equals H_S (Eqn (1)). The porosities of snow and slush are considered equal, and the maximum slush density (ρ_{slmax}) can be calculated

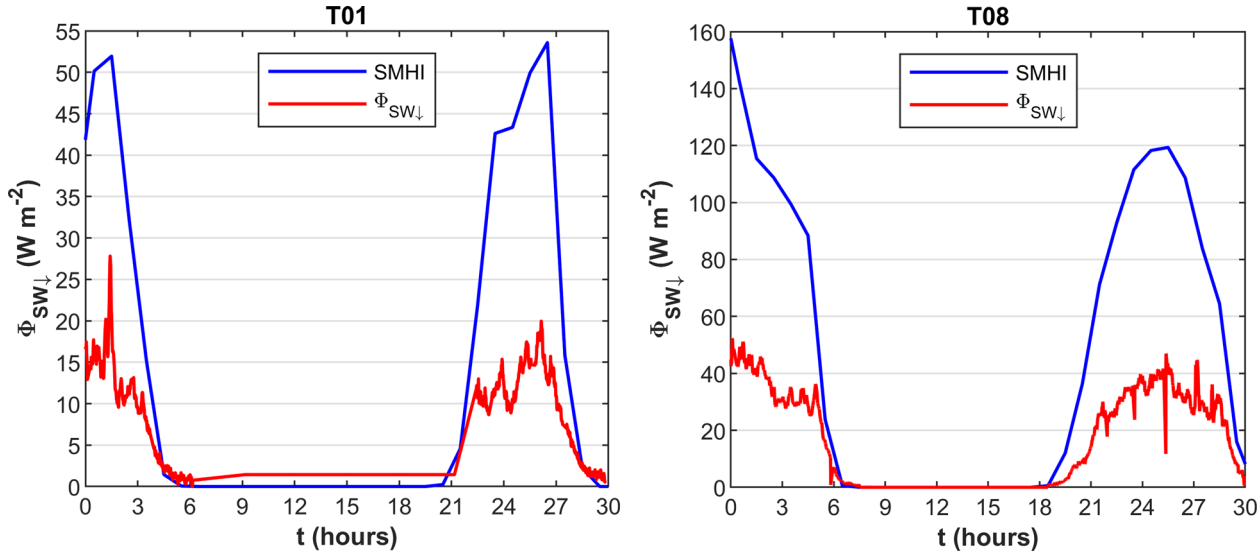

Figure 9. Incoming solar radiation ($\varphi_{SW\downarrow}$) measured at the SMHI meteorological station (airport Luleå) is indicated by the solid blue line and the solar radiation measured at the tank during the first and last experiments is shown by a solid red line. Midnight corresponds to $t = 14$ h.

https://doi.org/10.1017/aog.2023.58 Published online by Cambridge University Press

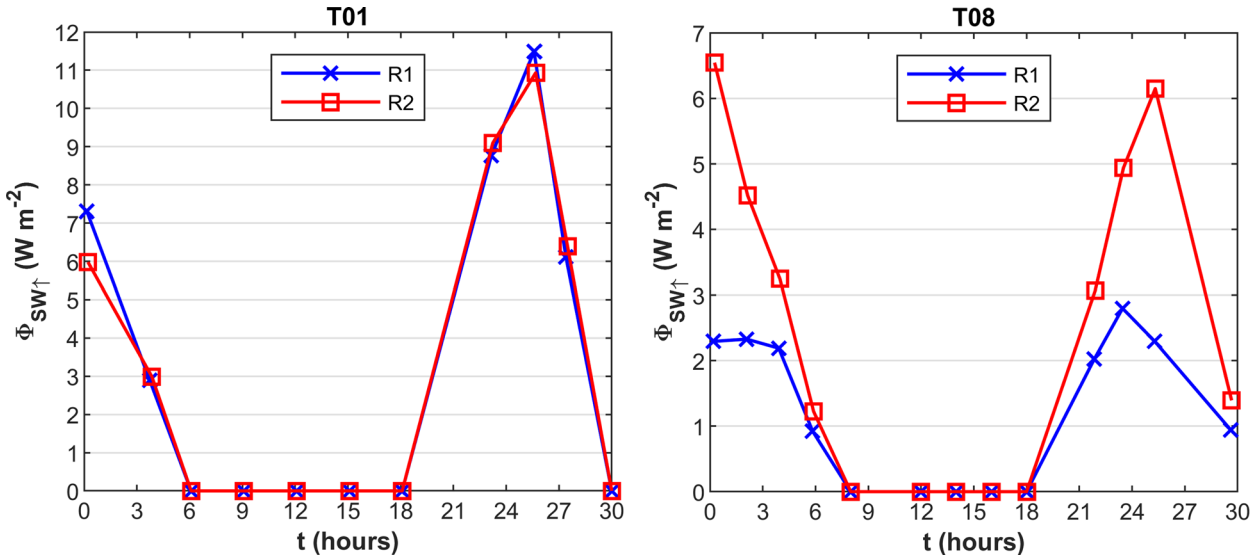

Figure 10. The reflected solar radiation measured during the first and last experiments. The red and blue lines show the reflected radiation from the ice surface in the first and second compartments (R1 and R2), respectively. Midnight corresponds to $t = 14$ h. Note that the reflected radiation is similar in both snow-covered compartments in T01 after 4 h, while it is higher for bare snow ice (R2) compared to the bare congelation ice in T08R1.

from:

$$\rho_{sl\,\max} = \rho_w - \rho_s\left(\frac{\rho_w}{\rho_i} - 1\right), \tag{2}$$

where subscripts *sl*, *s*, *w* and *i* stand for slush, snow, water and ice. The density of fresh water ice (ρ_i) is 917 kg m^{-3} (Cox and Weeks, 1983).

When snow submerges in water, the 'warm' water, and the 'cold' snow exchange heat. In a closed system, the specific heat flux will approach zero when slush and water reach temperature equilibrium (e.g., Lei and others, 2014). Depending on the heat content some slush may transform into water or SI. The fraction of ice that may melt or freeze can be estimated by considering mass and energy conservation balance within a closed system. This estimation assumes that the heat exchange between the submerged snow and water, until temperature equilibrium is reached, is not influenced by the simultaneous heat exchange at slush/atmosphere and slush/water interfaces. This assumption is valid when temperature equilibrium is reached quickly.

The net energy balance (E) between snow and water is equal to the sum of energy released from water cooling (E_w) and the energy consumed from warming the snow, E_s. A positive E suggests that the excess energy goes into melting slush while a negative balance suggests the freezing of slush. The net energy balance is as follows:

$$E = H_w\rho_w c_w(T_w - T_{SL}) + H_s\rho_s c_s(T_S - T_{SL}). \tag{3}$$

where $c_w = 4217$ J kg^{-1}°C^{-1} (Incropera and others, 2007) and $c_s = 2117$J kg^{-1}°C^{-1} (Mellor, 1977) are the specific heat capacities of water and snow, respectively. If the slush equals the theoretical snow thickness, then the water thickness (H_W) can also be considered equal to H_S. (T_W-T_{SL}) and (T_S-T_{SL}) are the temperature gradients (ΔT_W and ΔT_S) between the initial water (T_W) and snow (T_S) temperatures with the slush temperature (T_{SL}) in

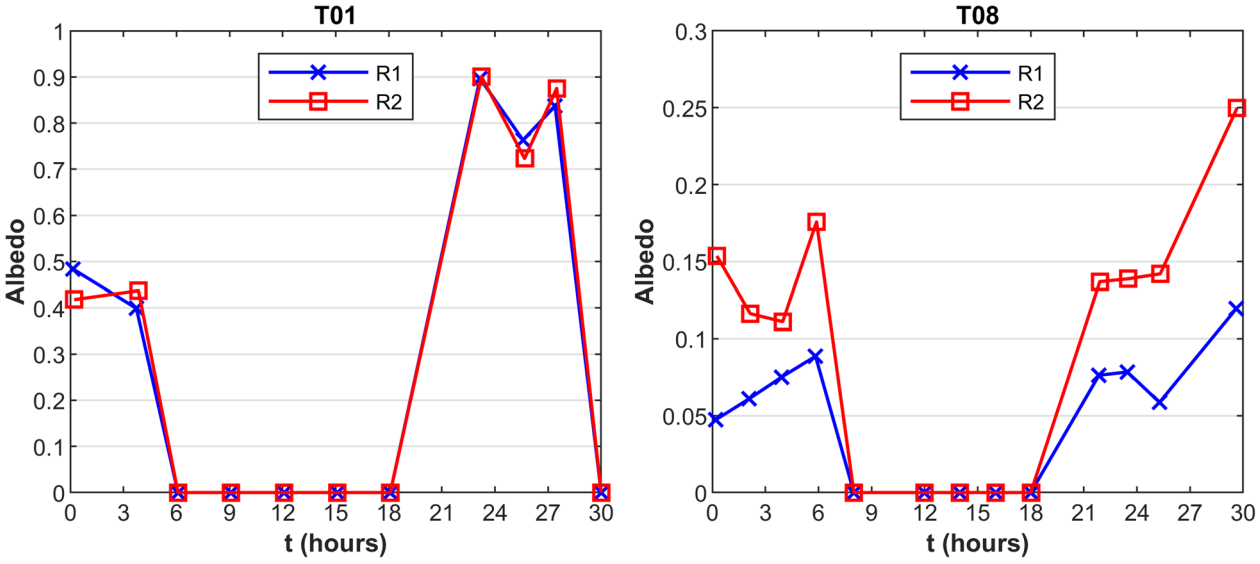

Figure 11. The albedo measured from the different compartments during the first (T01) and last (T08) experiments of C2. Note how the albedo of the bare snow ice in compartment R2 in the last experiment (T08) is visibly higher than the albedo of bare congelation ice in R1.

https://doi.org/10.1017/aog.2023.58 Published online by Cambridge University Press

equilibrium. Snow temperature and air temperature are assumed to be equal.

After snow submersion in water, the excess energy will melt a fraction of the ice crystals, thus increasing the water content (porosity) in the slush layer and melting the slush at the water/slush interface. The deficiency of energy will increase the slush porosity by merging and freezing into SI. Presuming that the fraction of slush that melts and freezes in the pores equals a representative equivalent thickness change (ΔH_{SL}), this is equal to:

$$\Delta H_{SL} = \frac{E}{\rho_{sl} L_i}, \tag{4}$$

where L_i is the latent heat of ice formation (3.34.105 J kg^{-1}). In the current study, ρ_{slmax}, and slush densities of 600, 700, 800 and 900 kg m^{-3} (Weeks and Lee, 1958) are used in estimating ΔH_{SL}. Assuming that the slush porosity is equal to the snow porosity ($p_{sl} = p_s = 1 - \rho_s/\rho_i$) and the initial slush thickness (H_{SL}) equals the theoretical H_S, the instant slush porosity (Δp_{SL}) reduction or increase is:

$$\Delta p_{sl} = \frac{\Delta H_{SL0}}{p_s H_S}. \tag{5}$$

The assumption that H_{SL0} equals H_S neglects possible instant occurrences such as crystal agglutination or separation. These processes may lead to instant snow compression or expansion, respectively.

In a companion study, 20 experiments were performed to investigate the initial thickness of slush that was formed from snow submergence in a transparent container (Zhaka and others, 2022). This study statistically analysed the effect of the initial snow mass or theoretical thickness, initial snow temperature and water temperature in the slush thickness (H_{SL0}) instantly after the submergence. A linear regression equation that determined the H_{SL0} as a function of the theoretical H_S was obtained (Zhaka and others, 2022), and was used here to estimate the H_{SL0} for the C1 series of experiments as well as C2T01.

4.2 Water and slush freezing

The ice growth is estimated from two simple models. The first model (Stefan, 1889) neglects the surface heat budget, the water heat flux, the snow layer and the thermal inertia. The air and ice surface temperatures are considered equal ($T_A = T_S$), and the ice growth equation is derived from the continuity equation at the ice/water interface. The ice thickness, H, is given by:

$$H = a\theta^{0.5}, \tag{6}$$

where Stefan's growth rate coefficient (a) in mm°C$^{-0.5\ -0.5}$ is

$$a = \sqrt{\frac{2k_i}{\rho_i L_i}}, \tag{7}$$

and the cumulative freezing air temperatures (θ in °C d) equates:

$$\theta = \int_0^t (T_F - T_A)\mathrm{d}t. \tag{8}$$

T_F is the freezing temperature of fresh water (0°C).

The second model (Ashton, 1986, 1989) considers the heat exchange at the ice/atmosphere interface and the water heat flux (φ_w) at the ice/water interface. The ice growth model for CI is:

$$\frac{\mathrm{d}H_I}{\mathrm{d}t} = \frac{1}{\rho_i L_i} \frac{T_F - T_A}{(H_I/k_i) + (1/h_{ia})} - \frac{\varphi_w}{\rho_i L_i}. \tag{9}$$

The value of the pure ice heat conductivity k_i at the freezing temperature is assumed equal to 2.07 W m^{-1}°C^{-} (Yen, 1981). The convective heat transfer coefficient h_{ia} (in W m^{-2} °C) at the ice/air interface is determined by fitting the model with all the measured thicknesses of CI.

The estimation of SI from freezing slush assumes a $\varphi_w = 0$ at the SI /slush interface. When estimating the CI formation under the SI the water heat flux is considered. The thickness of SI (H_{SI}) for initial conditions of ($H_{SI0} = 0$) at $t = 0$ is:

$$\frac{\mathrm{d}H_{SI}}{\mathrm{d}t} = \frac{1}{\nu_w \rho_{si} L_i} \frac{T_F - T_A}{(H_{SI}/k_{si}) + (1/h_{si})} - \frac{q_w}{\nu_w \rho_{si} L_i}. \tag{10}$$

The naturally formed slush has a density lower than ρ_{slmax} (Weeks and Lee, 1958), because the air pores present in the snow are partly replaced by water. Thus, the SI density (ρ_{si}) is assumed equal to 900 kg m^{-3} (Ager, 1962). SI with a bulk density equal to 900 kg m^{-3} has a snow-ice conductivity coefficient (k_{si}) equal to 2.03 W m^{-1} °C^{-1} (Schwerdtfecer, 1963). The convective heat transfer coefficient in the snow-ice/air interface (h_{sia}) is determined by the model fit with all the measured SI thicknesses. The SI growth equation assumes that the freezing takes place only in the water filled voids present in the slush layer. Assuming that the water fraction (ν_w) in the slush layer is equal to the air fraction (ν_a) in dry snow than, ν_w is:

$$\nu_w = \left[1 - \frac{\rho_s}{\rho_i}\right]. \tag{11}$$

The analytical solution that considered the dry snow and the snow/atmosphere coupling effect adds in the above models (Eqns (9 and 10)) the equivalent heat transfer coefficient (h_e) from the snow layer to the atmosphere:

$$h_e = \frac{H_S}{k_s} + \frac{1}{h_{sa}}. \tag{12}$$

For a snow density ρ_s equal to 200 kg m^{-3}, the snow thermal conductivity k_s is equal to 0.1034 W m^{-1} °C^{-1} (Yen, 1981). The convective heat transfer coefficient h_{sa} at the snow/air interface differs from h_{ia}, which is the case when the snow layer is neglected.

In the current study, the thickness estimations were carried out considering: (1) all the CI measured from different experiments; (2) all SI measurements for the duration where only SI was freezing from slush; (3) all experiments where CI was formed under SI. The water heat flux was considered when estimating the CI thickness, but it was neglected when estimating the SI growth. The insulative effect of the slush layer underneath the freezing boundary was considered instead. Three different formulations for calculating the water heat flux are elaborated in the supplementary material: (1) where φ_w was estimated from the heat flux budget at the ice/water interface (Purdie and others, 2006; Lei and others, 2014, 2018); (2) the molecular conductivity earlier applied by Sengers and others (1984); and Ramires and others (1995); (3) the parameterised equation earlier used in lake ice estimations (Shirasawa and others, 1997, 2006; Ohata and others, 2016). In the current data analysis, we used φ_w calculated from molecular conductivity formulation.

https://doi.org/10.1017/aog.2023.58 Published online by Cambridge University Press

Table 2. Snow mass (m_s), theoretical snow thicknesses (H_S), estimated initial slush thickness (H_{SL0e}) from Eqn (3), measured initial slush thicknesses (H_{SL0m}), temperature differences (ΔT_w) between initial T_W and T_{SL} at equilibrium, slush equivalent thickness (Δ_{HSL0}) and porosity changes (Δp_{sl}) at temperature equilibrium

Experiment ID	m_s kg	ΔT_w °C	H_S mm	H_{SL0e} mm	H_{SL0m} mm	Δ_{HSL0} mm	Δp_{sl} %
C1-T01 R2	6.9	2.9	98	113	–	2.9	3.4
C1-T03 R2	2.5	1.8	41	52	–	1	2.8
C2-T01 R1	3	1.8	28	38	–	0.2	0.7
C2-T02 R1	6	1.4	91	104	113	1.6	2.1
C2-T03 R2	1.5	0.5	22	31	25	0.1	0.5
C2-T04 R2	4.5	0.4	59	70	70	−0.4	−0.7
C2-T05 R2	6	2.2	75	87	80	2	3.1
C2-T06 R1	1.5	1.4	27	36	30	0.4	1.7
C2-T07 R1	4.5	0.4	60	72	75	0.3	0.6
C2-T08 R2	3	0.4	39	49	40	0.1	0.3

5. Data analysis

In the following subsections, the initial slush thickness and the phase transition in the slush/water interface are assessed. The thickness of SI formed from the initial slush thickness is also analysed. Furthermore, the freezing rate of slush is compared to the freezing rate of water and the CI growth under the SI layer is compared with CI growth under CI. The albedo differences between slush and water; and between SI and CI are presented.

5.1 Snow to slush transformation

The theoretical snow thicknesses (H_S), the estimated initial slush thickness (H_{SL0e} from Eqn (3)), and the measured initial slush thicknesses (H_{SL0m}) introduced in Section 3 are summarised in Table 2. H_{SL0m} are plotted against the theoretical snow thicknesses, see Figure 12. The linear regression equation (H_{SL0m} vs H_S) indicates that the snow expanded when submerged in water, the same behaviour was also reported earlier (Zhaka and others, 2022).

The temperature gradient between the snow and water leads to the melting or freezing of slush in the water-filled pores as well as at the water/slush interface. This initial slush transformation was expressed in Section 3 as an equivalent thickness change ΔH_{SL} (Eqn (5)), and slush porosity change Δp_{SL} (Eqn (6)). The ΔH_{SL} and Δp_{SL} were calculated for different slush densities within the interval of 600 kg m^{-3} to ρ_{slmax}. The decrease of the slush density from its maximum to 600 kg m^{-3} increased the ΔH_{SL} from 2.2 to 3.8 mm in C1T01. Also, the instant change of slush porosity increased when decreasing the ρ_{sl}. The ΔH_{SL} and Δp_{SL} given in Table 2 are calculated for a slush density equal to 800 kg m^{-3}. This density value was presumed a reasonable approximation considering the values reported in the literature between 600 and 850 kg m^{-3} (e.g., Weeks and Lee, 1958). These slush densities indicate that not all the air pores are replaced with water when snow submerges, but instead air pores remain in the slush (Colbeck, 1997).

After the snow submersion, the surface thermocouples recorded a temperature decrease (ΔT_w) of 2.9°C, and 1.8°C for C1T01 and C1T03, respectively. These ΔT_w correspond to a porosity increase (Δp_{SL}) of 3.4 and 2.8%. In C1T02R1, the initial temperature decrease was not recorded due to a restart error of the temperature logger.

In the second campaign, the surface thermocouples recorded the temperature peak caused by snow submergence in all the experiments, except for T04. The ΔT_w recorded at 50 mm depth is given instead in Table 2. The ΔT_w after the snow submergence varied between 0.4 and 2.2°C in C2-T08 and C2-T05, corresponding to Δp_{SL} of 0.3 and 3.1%. In C2-T04, the results indicate SI formation and an instantaneous decrease in porosity of 0.7%. This decrease was caused by the low-temperature gradient (0.4°C) between the initial water temperature and equilibrium slush temperature, and a higher temperature gradient (12.4°C) between the initial snow temperature and the equilibrium slush temperature. The calculated values of ΔH_{SL} are negligible compared to the measurement errors present in the initial slush thickness.

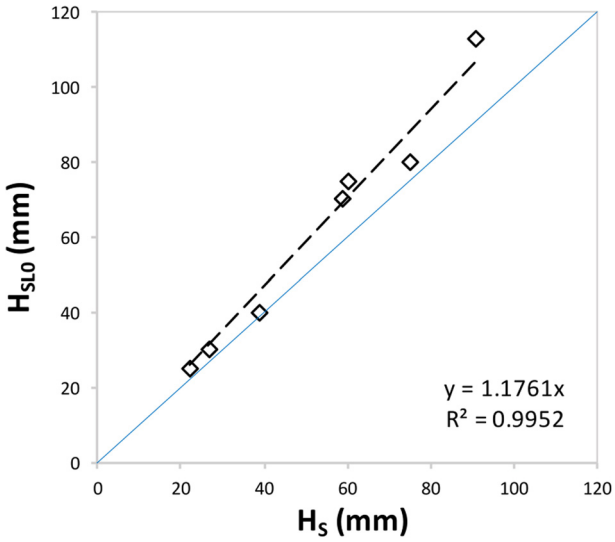

Figure 12. Measured initial slush thicknesses (H_{SL0}) for seven experiments (C2T02 to C2T08) plotted against the theoretical snow thickness (H_S). The regression dashed black line indicates that the snow expanded when submerged in water. The blue solid line shows H_S vs H_S (1:1 line).

Theoretically, the instantaneous change in porosity until temperature equilibrium also occurs when SI forms in the other two mechanisms, in snow/ice interface flooding (Knight, 1988) or the snow-ice formation initiated by precipitation. In these cases, the temperature difference between snow and seawater or precipitation water determines the occurrence of melting or freezing in the slush layer.

5.2 Initial phase transition at the slush/water interface

After the snow addition in the first campaign (C1), the surface thermocouples were submerged at the slush/water interface and recorded the temperature history at this interface. This provided qualitative insight regarding the heat exchange and phase transition between the snow, slush and water phases. The temperature recordings for the first 30 min of C1-T01 and C1-T03 (see Fig. 12) were interpreted based on the ice-water phase transition principles (Demirbas, 2006).

The snow-slush-water initial transition underwent four main stages after snow submersion, see Figure 13a. The first stage was the temperature drop caused by the snow addition in the water, which lasted two minutes. The second stage was a period of constant temperature, during which the slush-water phase change occurred. This phase lasted four minutes and melted a slush equivalent thickness of 2.9 mm. In the 3rd stage, the interface layer reached the temperature equilibrium 4 min after the snow addition. In the last stage, the water temperature increased, due to the temperature difference between the bottom of the tank and the slush/water interface. This temperature increase suggests that the slush/water interface moved upwards as the slush melted or compressed with time due to buoyancy.

https://doi.org/10.1017/aog.2023.58 Published online by Cambridge University Press

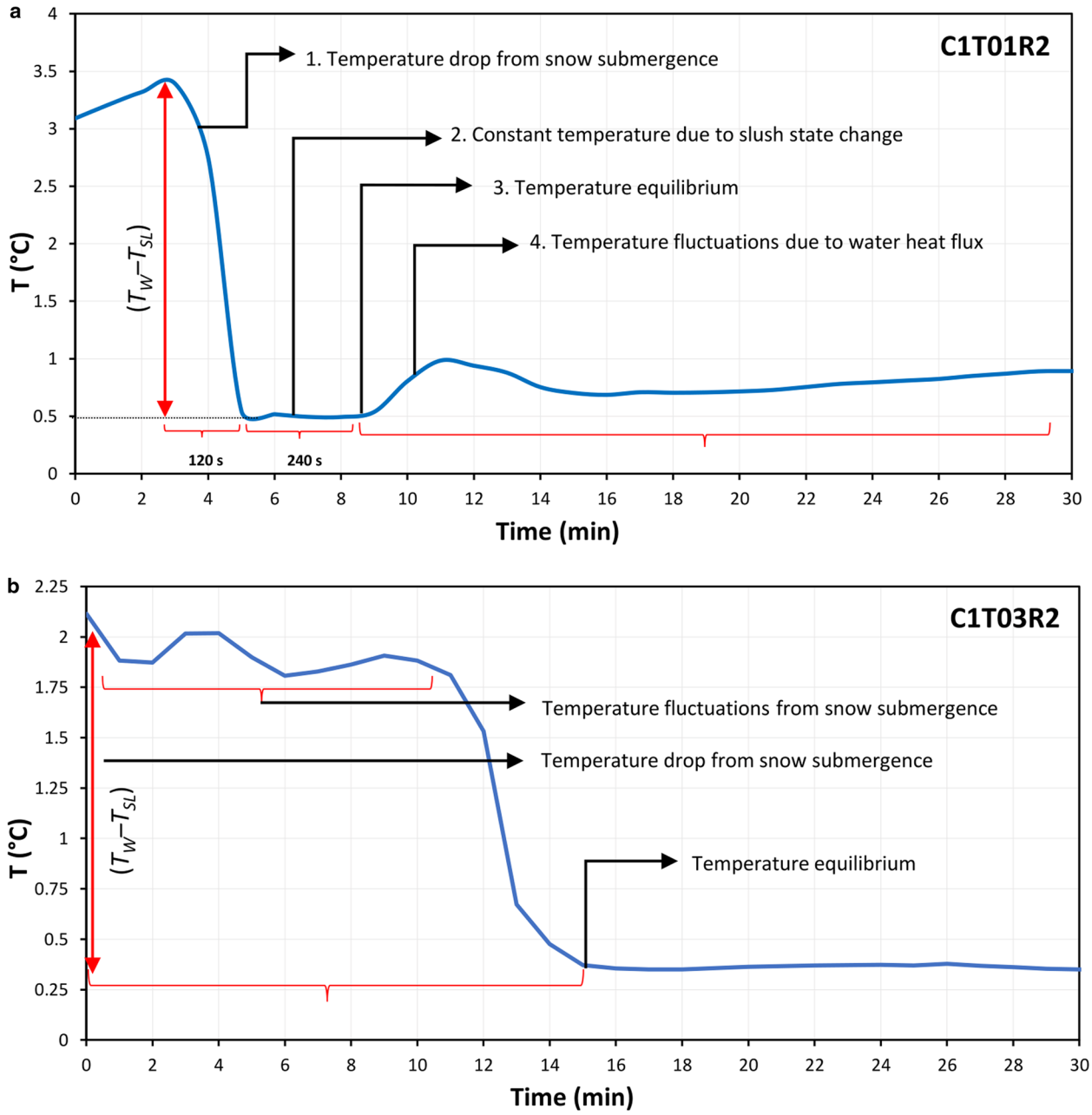

Figure 13. Temperature recordings at the slush/water interface for the first 30 min of C1T01R2 (a) and C1T03R2 (b).

During C1-T03, the snow addition was not instantaneous. Slower snow submersion in water caused a temperature fluctuation and elongated the first stage of the temperature drop, see Figure 13b. The phase change stage and the increase in the water temperature due to water heat flux cannot be precisely separated. These two phases are distinguished by the equilibrium temperature, which was reached instantly. The temperature equilibrium was reached instantly also in all C2 experiments.

5.3 Slush transformation to snow-ice

In the current study, only about 35% of the initial snow thickness or 30% of initial slush thickness transformed into SI, see Figure 14. The slush-snow ice transformation ratio (H_{SL0}/H_{SI}) was found to be 3.2 with a std dev. of 0.7. The regression equation given in Figure 14. can be used to estimate the thickness of SI based on the initial snow or slush thicknesses. Ice crystals are less dense than the water, consequently, the slush layer might be compressed under its own buoyancy, reducing its initial thickness and porosity. However, the extent to which the slush can compress and the duration of this process remain unclear.

In the current experiments, the initial slush thickness is bounded by air and water and the phase change can take place at both boundaries simultaneously. Assuming that the slush is at freezing temperatures throughout, SI will initially form at the slush/air interface and will continue to grow downwards as heat is released into the atmosphere. At the same time, a water column with a positive temperature gradient will generate a water heat flux, which can melt the slush at the slush/water interface. The freezing and melting of slush at the upper and lower interfaces continue until the slush layer completely transforms into SI or is completely melted. Note that slush compression and melting might occur at the same time. However, from the current experiments, the compression rate due to buoyancy cannot be addressed and slush reduction with time is attributed only to the melting process. Therefore, about 70% of the slush melted due to water heat flux or compressed due to buoyancy.

https://doi.org/10.1017/aog.2023.58 Published online by Cambridge University Press

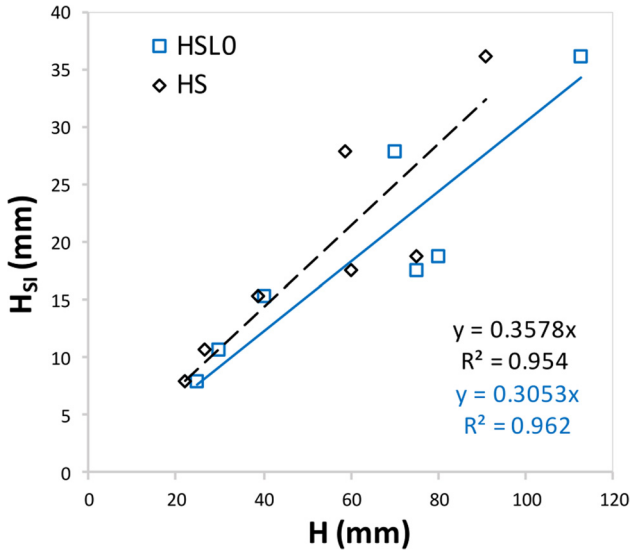

Figure 14. The total snow ice thickness (H_{SI}) formed in seven experiments (C2T02 to C2T08) is given as a function of the measured initial slush thickness (H_{SLO}) and theoretical initial snow thickness (H_S). The regression equations and goodness of fit for H_{SLO} vs H_{SI} and H_S vs H_{SI} are given with blue and black font, respectively.

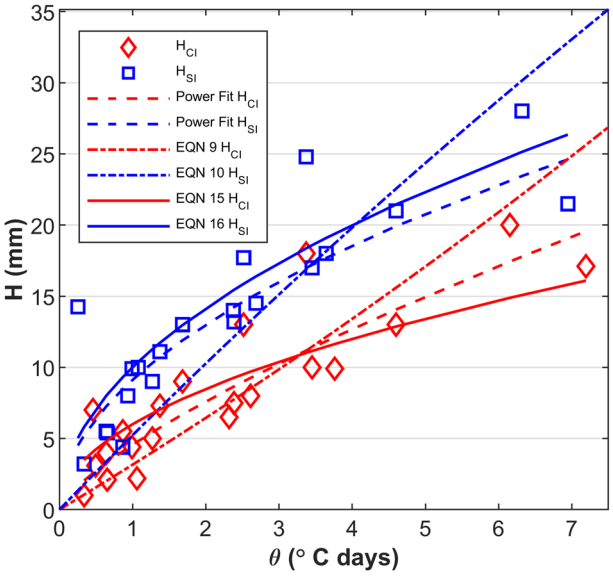

Figure 15. The measured and estimated thicknesses of congelation (CI) and snow ice (SI) are plotted against the cumulative freezing air temperatures (θ). The measured thicknesses of congelation ice (*HCI*) and snow ice (*HSI*) in the first campaign (C1) and the first 12 hours of the second campaign (C2) are given with red diamonds and blue squares, respectively. The best power trendline fits for both CI and SI are given with dashed red and blue lines. The estimated thicknesses of CI and SI from Stefan's (1889) Eqns (15 and 16) are illustrated with solid red and blue lines, while Ashton's (1989) model fits (Eqns (9 and 10)) are illustrated with dotted red and blue lines for CI and SI respectively.

Earlier studies of snow-ice formation in nature have reported different snow-slush-snow ice transformation ratios. For example, the transformation ratio of snow to slush in the snow/ice interface was 2/3 of the initial snow layer above the ice, and only half of the slush layer transformed to SI (Leppäranta and Kosloff, 2000), while elsewhere for the same mechanism, 1/3 of the initial snow layer on lake ice transformed to slush due to interface flooding (Knight, 1988). Ohata and others (2016) showed that half of the maximum snow thickness over the ice transformed into SI.

5.4 Snow ice and congelation ice growth

SI, slush and water were present in the SI experiments during the first campaign (C1), while in the second campaign (C2), CI began to form under the SI after approximately 12 h. The snow-ice and CI thicknesses (H_{SI} and H_{CI}) measured during C1 and the one measured during the first 12 h of each experiment in C2 are plotted against the cumulative freezing air temperatures (θ in °C d) in Figure 15. This figure shows the best power trendline fit, Stefan's (1898) and Ashton's (1989) models (see Section 3 Eqns (6, 9 and 10)). The scatter in thicknesses was mainly a result of uncontrolled environmental conditions.

The power regression equation that fits best the measured SI and CI thicknesses are (see Fig. 15):

$$H_{CI} = 4.55\theta^{0.74}, \quad (13)$$

$$H_{SI} = 9.11\theta^{0.51}. \quad (14)$$

These trendlines showed a difference of 6 mm between H_{SI} and H_{CI} for a θ equal to 7°C d. The correlation coefficients were equal to 0.78 and 0.76 in Eqns (13 and 14), respectively. The power exponent in the snow-ice formation (0.51) is closer to the one proposed by Stefan (1889) for the ice growth (0.5). The exponent that best fits the CI thickness measurements is larger (0.74). This is close to the exponent given by Ashton's (1989) ice growth formulation. These exponents suggest that the SI growth rate decreased quicker with increasing θ compared to CI.

Fitting Stefan's (1889) ice growth formulation results in the following equations:

$$H_{CI} = 6\theta^{0.5}, \quad (15)$$

$$H_{SI} = 10\theta^{0.5}, \quad (16)$$

where the values 6 and 10 are Stefan's ice growth rate coefficient in mm°C$^{-0.5}$ d$^{-0.5}$ (Eqn (7)). Based on this formulation the SI grew 4 mm faster than the CI, and for a maximum θ equal to 7°C d the SI was 10 mm higher than CI.

The estimation of CI growth with Ashton's (1989) Eqn (9) included a water heat flux term but was neglected when estimating the SI growth. The CI thickness was estimated using the maximum water heat flux estimated from all the experiments, which varied between 72 and 2.4 W m^{-2}. Ashton's (1989) ice growth formulation gave the best fit for SI and CI thicknesses when air/ice heat convective coefficients were 16 and 18 W m^{-2} °C^{-1}. This difference between h_i and h_{si} suggests that higher heat is conducted through the CI than the SI, which is attributed to the water heat flux term added in the H_{CI}. When the water heat flux term is omitted from Ashton's model then h_i equals 13 W m^{-2} °C^{-1}.

5.4.1 Total thickness (SI + CI)

For the second campaign (C2), the total thickness (H_T) represents the initial SI thickness formed from freezing all the slush within the first 12 h, and thereafter it is the sum of the SI and CI thickness formed underneath it. Figure 16 shows all the ice thickness measurements including the snow-covered and bare ice, together with the best power trendline fit, and Stefan's (1889) and Ashton's (1989) model fits.

Stefan's (1889) equation gave a growth rate coefficient equal to 8 and 11 mm°C$^{-0.5}$ d$^{-0.5}$ for H_{CI} and H_T, respectively. For θ equal to 18°C d the difference between H_{CI} and H_T reached up to 13 mm. The reduction in the growth rate by 1 mm when comparing

https://doi.org/10.1017/aog.2023.58 Published online by Cambridge University Press

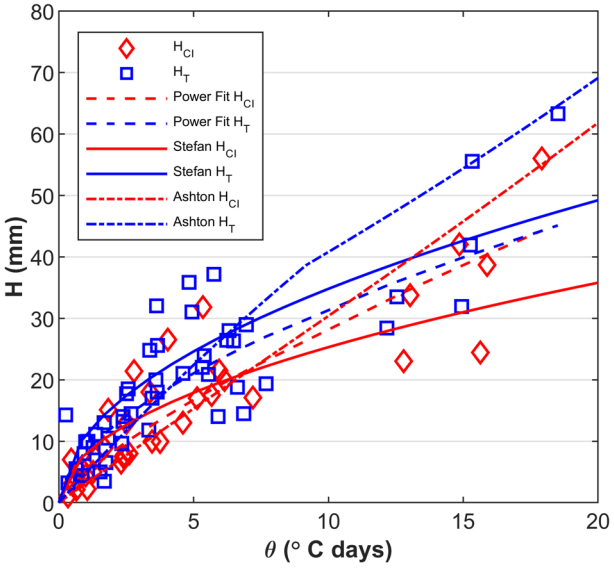

Figure 16. The measured and estimated congelation ice (H_{CI}) and total ice thicknesses and (H_T) are plotted against the cumulative freezing air temperatures (θ). The measured thicknesses of congelation ice (H_{CI}) and total thicknesses of the snow ice experiments (H_T) of the second campaign (C2) are given with red diamonds and blue squares. The best power trendline fits for both H_{CI} and H_T are given with dashed red and blue lines. The estimated H_{CI} and H_T with Stefan's (1889) model is illustrated with solid red and blue lines, while Ashton's (1989) model fits are illustrated with dotted red and blue lines.

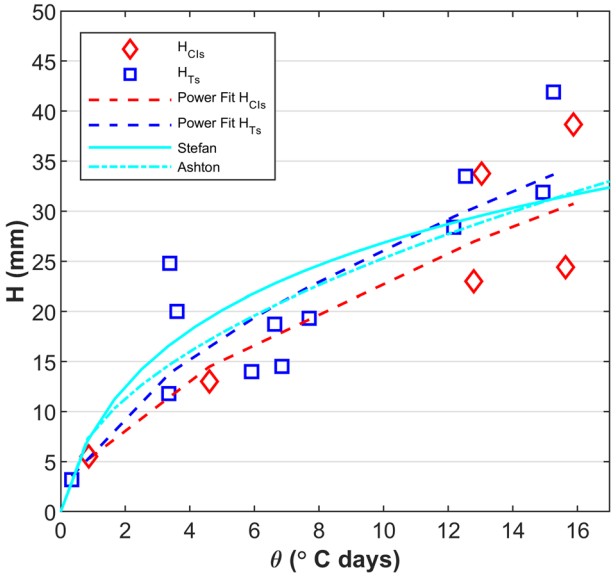

Figure 17. The measured and estimated thicknesses of snow-covered congelation ice (H_{CIs}) and snow-covered CI + SI (H_{Ts}) are plotted against the cumulative freezing air temperatures (θ). The snow-covered CI and CI + SI thicknesses are illustrated with red diamonds and blue squares. The dashed red and blue lines illustrated the best power trendline fit with the measured values. Stefan's (1898) and Ashton's (1989) model fits are illustrated with a solid and dotted cyan lines, respectively. Note that the same model lines fit all snow-covered thicknesses (H_{CI} and H_T).

H_{CI} with H_{SI} and H_{CI} with H_T may indicate that CI under CI forms faster than CI under SI.

Also, the best-power fit equation for H_{CI} crosses the equation for H_T at approximately 17°C d. This suggests that initially the SI + CI had a higher thickness due to the quick initial growth of SI, but when $H_{SL} = 0$, the CI growth under CI was slightly quicker than the CI growth under SI. It is probable that after H_{CI} equals the H_T (SI + CI), the H_{CI} exceeds the H_T. The current results are limited only to the number of cumulative air freezing temperatures where H_{CI} approached H_T but did not exceed it.

When estimating H_T, the water heat flux (φ_w) was assumed zero during SI growth and between 37 and 2.4 W m^{-2} when CI formed under SI (from the maximum calculated water heat flux). The addition of φ_w after $t = 12$ h and $\theta = 9$°C d (when estimating CI growth under SI) changes the slope in Ashton's model, see Figure 16. The ice growth models gave the best fit for H_T and H_{CI} using the air/ice heat convective coefficients (h_i) equal to 17 and 18 W m^{-2} °C^{-1}. As expected, the heat transfer coefficient in this case of H_T is the average value between the one estimated for SI and CI, see Figure 15.

5.4.2 Snow-covered ice

Figure 17 illustrates the measured snow-covered ice thicknesses (H_{CI} and H_T). The power trendline fits for H_{CI} and H_T have almost similar power exponents close to 0.6 and a difference in the growth rate coefficient equal to 1 mm°C$^{-0.5}$ d$^{-0.5}$, see the power equations given in Figure 17. Stefan's (1989) growth model fits both snow-covered thicknesses H_{CI} and H_T for a growth rate coefficient equal to 8 mm°C$^{-0.5}$ d$^{-0.5}$. Ashton's (1989) model fits all the snow-covered thicknesses (H_{CI} and H_T) for the same snow/air convective heat transfer coefficient (h_s) of 30 W m^{-2} °C^{-1}. The snow/air convective heat transfer coefficient results were considerably higher than the convective heat transfer coefficients at the CI/air and SI/air interfaces (18 and 16 W m^{-2} °C^{-1}).

5.5 Congelation ice growth under snow ice

The rate of water freezing under a SI layer is being compared to the rate of water freezing under a CI layer. The thickness of the CI (ΔH_{CI}) formed under the existing CI layer in a time interval Δt is equal to $H_{CI\,(t+\Delta t)} - H_{CI\,(t)}$, where t is the time of measurement. The CI thickness (ΔH_{CIs}) formed under the existing SI layer is equal to $H_{CIs\,(t+\Delta t)} - H_{Cis\,(t)}$, for the same time interval (Δt) as the CI measurements. These thickness differences are plotted against the difference in cumulative air freezing temperatures ($\Delta\theta = \theta_{(t+\Delta t)} - \theta_{(t)}$) for the same time interval (Δt), as shown in Figure 18. Even though the data of ΔH_{CIs} vs $\Delta\theta$ include scatter, the linear regression equation fitted on the data illustrates that the difference between water freezing under CI and SI is small. Considering the power equation fit (ΔH_{CIs} vs $\Delta\theta$), the coefficient of growth rate between the CI growth under CI and SI differs with 1 mm°C$^{-0.5}$ d$^{-0.5}$. Also, the Stefan model fit in Figure 16 indicated that CI growth under SI was slightly lower compared to CI growth under CI.

5.6 Solar radiation

A representative albedo value for open water is 0.06. It is 0.52 for bare first-year ice, and for melting white ice the albedo may range between 0.56 and 0.68 (Perovich, 1996). A representative albedo value for refrozen white ice is 0.7 (Allison and others, 1993; Perovich, 1996). In the current study, the albedo measured in each compartment in the time interval of 0.2 to 3.3 h for open water/thin CI varied between 0.047 and 0.147 with an average of 0.09, see Figure 19a. The albedo of slush/slush-thin SI varied between 0.1 and 0.2 with an average of 0.15. These albedo values are the averages of the initial phase of formation without distinguishing between the albedo of water and thin ice or between slush and SI. The albedo difference between the bare ice surface of SI and CI ($\Delta a = a_{SI} - a_{CI}$) resulted in a positive albedo difference and increased with the increase the initial snow mass, as shown in Figure 19b.

The radiation heat flux absorbed or scattered by the total ice thickness for 30 h was simply determined from the extinction law of radiation considering extinction coefficient earlier presented by (Arndt and others, 2017) and radiation penetration coefficient after (Sahlberg, 1988). On average, the amount of

https://doi.org/10.1017/aog.2023.58 Published online by Cambridge University Press

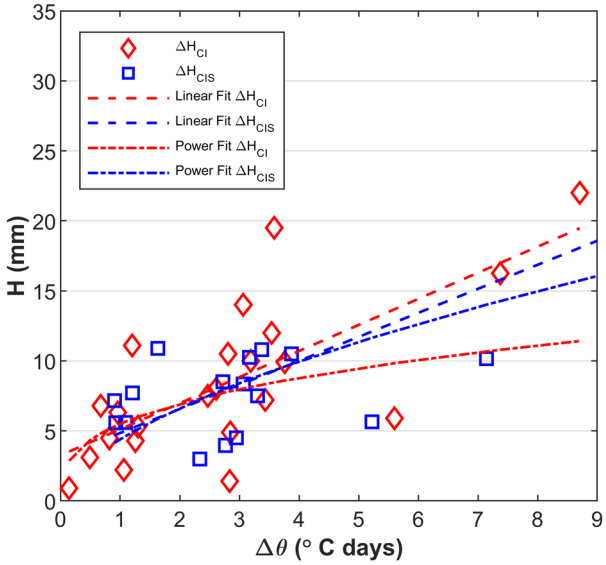

Figure 18. The measured thicknesses of the congelation ice (ΔH_{CI}) formed under the existing CI layer and the SI layer (ΔH_{CIS}) in a time interval Δt and plotted against the cumulative freezing air temperatures ($\Delta\theta$) for the same time interval (red diamonds and blue squares respectively). The best linear and power trendline fits are also illustrated with dashed and dotted red and blue lines for ΔH_{CI} and ΔH_{CIS}, respectively.

radiation that remained on ice varied between 0.6 to 2 W m^{-2}. Despite the higher albedo of SI compared to CI, the amount of radiation that was absorbed or scattered from the total ice thickness was slightly greater for H_T (SI + CI) compared to H_{CI}. This was a result of the higher thicknesses of (SI + CI) compared to the CI. For example, in the last experiment (C2T08), the CI had on average absorbed 0.83 W m^{-2} of solar radiation which corresponds to a temperature increase of 0.03°C. While in the other compartment where snow was submerged, the SI + CI had in average absorbed 1.14 W m^{-2} which correspond to an ice temperature increase of 0.034°C.

6. Discussion

When the snow was submerged in water, the temperature equilibrium was reached instantly, and the slush phase change in the water-filled pores and at the slush/water interface occurred instantly. A similar result was also reported in a saline slush formation laboratory study (Jutras and others, 2016). The initial slush thickness was found to be higher than the calculated submerged thickness, suggesting that snow expands when submerged in water close to the freezing point. This observation was also made earlier by Zhaka and others (2022).

If all the slush transforms to SI, then the total thickness (slush + snow ice) should remain constant over time. However, in the current experiments, the total thickness decreased with time. This decrease may be attributed to the compression of slush over time due to the buoyancy force, resulting in a reduction in both slush porosity and thickness. Additionally, slush melted at the water/slush interface due to water heat flux. It is possible that both phenomena occur simultaneously. However, in the current study, these phenomena cannot be distinguished.

A significant distinction between the SI formation observed in the current study and the SI formation resulting from level ice flooding is the presence of different boundary layers in the top and bottom of the slush. In the current experiments, the slush is initially bounded by air and water, whereas during SI formation due to flooding, the slush is bounded by dry snow or air and ice. This disparity in boundary conditions could explain the varying fractions of slush-to-snow ice transformation observed: approximately 0.3 in the present experiments vs 0.5 for SI formation by flooding (Leppäranta and Kosloff, 2000). Therefore, according to Figure 14 in the current study, it is evident that only about 30% of the initial slush thickness transformed into slush, and approximately 70% of the slush either melted due to water heat flux or compressed due to buoyancy.

The simple linear regression equations, illustrated in Figs 12 and 14, quantify the snow-slush-snow ice transformation. The first equation can estimate the initial slush thickness based on the theoretical snow thickness, and the second equation can estimate the total snow-ice thickness from the initial slush thickness. Both correlations can be used to estimate the SI formation by the first mechanism, where the SI forms from snowfall in freezing water in the early winter. Additionally, these simple equations can be used to evaluate the snow contribution to the total brash ice thickness formed in ship channels or ports.

For the same environmental conditions, it was observed the initial formation of SI from freezing slush was quicker than the initial ice growth from freezing water (CI). Stefan's model gave

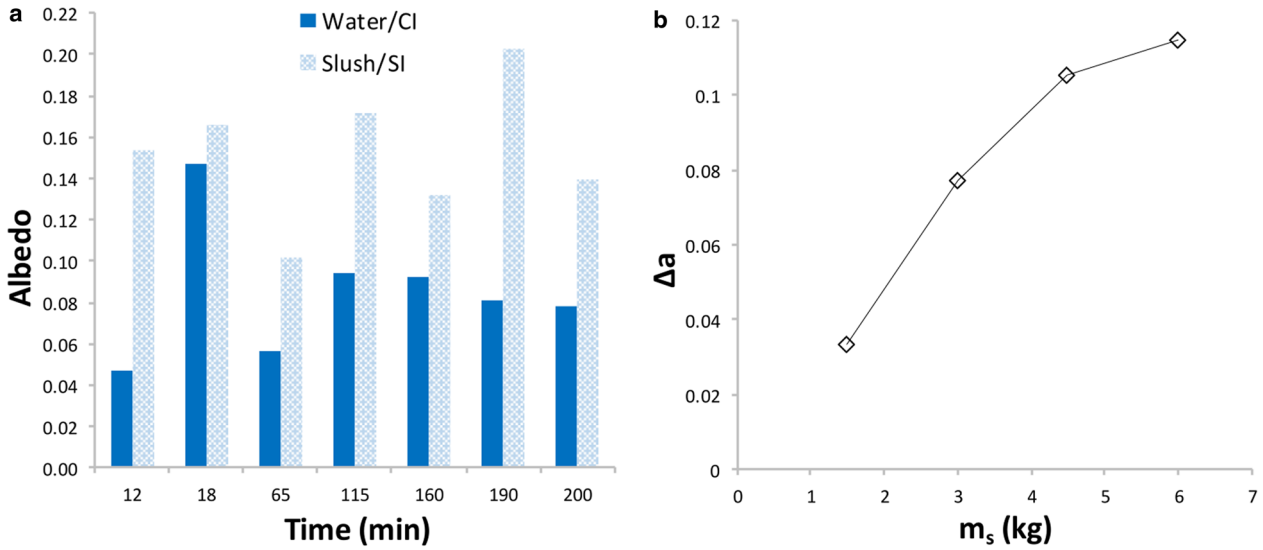

Figure 19. (a) Measured albedos at the beginning of each experiment. The blue bars illustrate the open water or thin congelation ice (CI) albedos, while the patterned light blue bars show the slush surface or thin snow ice (SI) albedos. (b) The difference in average albedo (Δa) between SI and CI in T02, T03, T04 and T08 vs the initial snow mass submerged in water.

https://doi.org/10.1017/aog.2023.58 Published online by Cambridge University Press

a growth rate difference between SI and CI equal to 4 mm°C$^{-0.5}$ d$^{-0.5}$. The quicker formation of SI compared to CI, can be attributed to several phenomena: (1) the slush only freezes in the water pores; (2) the temperature gradient in the slush layer is theoretically zero and (3) less solar radiation reaches the snow ice-water system due to a higher surface albedo of the SI compared to CI.

Thus, the slush beneath the freezing boundary (SI/slush) acts as insulation, preventing direct contact between the warm water and the freezing interface. In contrast, in the case of CI formation, the water is in direct contact with the freezing interface and provides heat, which can reduce or sometimes prevent the ice growth. During SI formation from slush, the water's heat flux melts the bottom of the slush layer. This explains why only about 30% of the initial slush layer transformed into slush.

Additionally, the albedo measured in open water/thin CI gave an average value of 0.09, while the albedo of slush/slush-thin SI averaged 0.15. The albedo difference between SI and CI was up to 0.12 (higher in SI). This albedo difference increased with increasing the mass of snow submerged in the water. This difference suggests that, for the same solar radiation intensity, the heat transmitted in CI/water interface is higher compared to the energy transmitted in the SI/slush interface.

However, the growth of CI under SI was slightly slower compared to CI growth under CI. The difference in the growth rate coefficient was estimated to be 1 mm°C$^{-0.5}$ d$^{-0.5}$ for a cumulative freezing air temperature of 9 °C d. This minor difference can be attributed to the varying conductive heat coefficients for the CI and SI. The presence of air pores within the SI lowers its conductivity from 2.07 W m^{-1}°C^{-1} for pure ice with a density of 917 kg m^{-3} (Yen, 1981) to 2.03 W m^{-1}°C^{-1} for SI with a density as high as 900 kg m^{-3} (Schwerdtfecer, 1963).

Despite the higher albedo of SI compared to CI, which may have affected the initial growth of SI, the absorbed radiation heat by the SI was higher compared to CI due to the thicker SI layer. This may have influenced the CI growth underneath SI and CI. However, a previous study of the thin ice growth initiated by snow submersion in the water suggested that the thickness of the SI layer did not significantly affect the subsequent ice growth rate (Toyota and others, 2020).

The estimated snow-ice growth rate in this study may have relevance for other snow-ice formation conditions and different mechanisms, such as the snow-slush-snow ice transformation that occurs in level ice from flooding and the transformation that is initiated by precipitation. In these cases, the slush is bounded by snow or air and by ice, which acts as insulation, protecting the slush from the water heat flux, while SI forms at the air/slush or snow/slush interfaces.

In the current study, the SI also formed at the air/slush boundary, and in a few experiments, snowfall also affected the ice growth. The slush beneath acted as insulation, protecting the SI from the water heat flux. This mechanism of slush transformation where the growth occurs at SI/slush interface while slush simultaneously melts at the slush/water interface, can be considered comparable to another process observed in drifting and coastal ice (Lytle and Ackley, 2001; Shirasawa and others, 2005), where the slush to SI transformation occurred simultaneously with the bottom melting of CI.

Conclusions

Congelation and snow-ice growth experiments were carried out in a fresh water tank exposed to the outdoor freezing temperatures at Luleå University of Technology facilities in Sweden, during two consecutive winters in 2021 and 2022. This study investigated the snow-slush-snow ice transformation. The initial snow-ice (SI) growth from freezing slush was compared with the CI growth from freezing water. The tank was divided into two compartments to conduct simultaneous experiments. In each experiment, in one compartment the snow-slush-snow ice transformation was observed and in the adjacent compartment water freezing was investigated. The first campaign consisted of four experiments, each lasting 8 h. In the second campaign, eight experiments were conducted, each lasting 30 h.

About 30% of the initial slush layer transformed into SI and about 70% either melted or compressed due to the buoyancy. This fraction can be considered when estimating the SI formation at the beginning of winter when the snowfall submerges in the water close to the freezing temperatures. These findings can be used to assess the significance of the snow-slush-snow ice transformation in determining the overall thickness of brash ice formed in ports and ship channels.

The SI growth from slush was 4 mm °C$^{-0.5}$ d$^{-0.5}$ faster compared to CI growth from water. This can be attributed to three main factors. Firstly, the slush freezes only in the pores, which accelerates the freezing process. Secondly, the slush layer acts as an insulator, preventing the direct contact of SI with water. Additionally, the higher albedo of SI compared to CI (an average difference of 0.12) results in lower absorption of solar radiation, leading to reduced energy gain.

However, CI growth under CI was 1 mm °C$^{-0.5}$ d^{-0}5 faster than CI growth under SI. This slight difference can be attributed to two factors. Firstly, the SI layer has a higher air content, which reduces the conductivity of SI compared to CI. Secondly, the initial thickness of SI is higher, resulting in slightly more solar energy absorption compared to CI.

This experimental setup provides an opportunity to further investigate and gain insights into the porosity and density transformation of snow-slush-snow ice, as well as these key parameters impact the thermodynamic properties and growth of SI in comparison with CI. Additionally, the same setup can be used to study the formation of SI resulting from flooding and melting processes.

Supplementary material. The supplementary material for this article can be found at https://doi.org/10.1017/aog.2023.58.

Acknowledgement. The authors would like to acknowledge the support from TotalEnergies, and the help received from the technicians and staff at the Luleå University of Technology.

Author contributions. VZh: Conceptualisation, planning the experiments, performing the experiment, data curation, data analysis, visualisation, writing the original manuscript, writing review and editing. RB: Conceptualisation, planning the experiments, performing the experiment, writing review and editing. KR: Conceptualisation, supervision, writing review and editing. AH: Hardware contributions, writing review and editing. AC: Conceptualisation, Supervision.

References

Adolphs U (1998) Ice thickness variability, isostatic balance and potential for snow ice formation on ice floes in the south polar Pacific Ocean. *Journal of Geophysical Research: Oceans* **103**(C11), 24675–24691. doi: 10.1029/98JC02414

Ager BH (1962) Studies on the density of naturally and artificially formed fresh-water ice. *Journal of Glaciology* **4**(32), 207–214. doi: 10.3189/s0022143000027404

Allison I, Brandt RE and Warren SG (1993) East Antarctic sea ice: Albedo, thickness distribution, and snow cover. *Journal of Geophysical Research: Oceans* **98**(C7), 12417–12429. doi: 10.1029/93JC00648

Arndt S and 5 others (2017) Influence of snow depth and surface flooding on light transmission through Antarctic pack ice. *Journal of Geophysical Research: Oceans* **122**(3), 2108–2119. doi: 10.1002/2016JC012325

Ashton GD (1974) Evaluation of ice management problems associated with operation of a mechanical ice cutter on the Mississippi river. CRREL

Special Report, US Army Cold Regions Research and Engineering Laboratory, (214).
Ashton GD (1986) River and lake ice engineering. *Water Resources Publications: U.S Library of Congress Catalog Number,* **2nd Edn**, 86–50681.
Ashton GD (1989) Thin ice growth. *Water Resources Research* **25**(3), 564–566. doi: 10.1029/WR025i003p00564
Ashton GD (2011) River and lake ice thickening, thinning, and snow ice formation. *Cold Regions Science and Technology* **68**(1–2), 3–19. doi: 10.1016/j.coldregions.2011.05.004
Cheng B and 6 others (2014) Evolution of snow and ice temperature, thickness and energy balance in Lake Orajärvi, northern Finland. *Tellus A: Dynamic Meteorology and Oceanography* **66**(1), 21564. doi: 10.3402/tellusa.v66.21564
Colbeck SC (1997) A review of sintering in seasonal snow, *CRREL Rep*. 97–10, *Cold Regions Research and Engineering Laboratory,Hanover, N. H.*
Cox GFN and Weeks WF (1983) Equations for determining the gas and brine volumes in sea ice samples. *CRREL Report, US Army Cold Regions Research and Engineering Laboratory* **29**(102), 306–316. doi: 10.3189/s0022143000008364
Demirbas MF (2006) Thermal energy storage and phase change materials: an overview. *Energy Sources, Part B: Economics, Planning, and Policy* **1**(1), 85–95. doi: 10.1080/009083190881481
Fichefet T and Maqueda MM (1999) Modelling the influence of snow accumulation and snow-ice formation on the seasonal cycle of the Antarctic sea-ice cover. *Climate Dynamics* **15**(4), 251–268. doi: 10.1007/s003820050280
Granskog MA, Vihma T, Pirazzini R and Cheng B (2006) Superimposed ice formation and surface energy fluxes on sea ice during the spring melt-freeze period in the Baltic Sea. *Journal of Glaciology* **52**(176), 119–127. doi: 10.3189/172756506781828971
Grenfell TC and Maykut GA (1977) The optical properties of ice and snow in the Arctic Basin. *Journal of Glaciology* **18**(80), 445–463. doi: 10.3189/S0022143000021122
Incropera FP, Dewitt DP, Bergman TL and Lavine AS (2007) *Fundamentals of Heat and Mass Transfer*, 6th Edn. Hoboken, NJ: John Wiley & Sons.
Jeffries MO, Krouse HR, Hurst-Cushing B and Maksym T (2001) Snow-ice accretion and snow-cover depletion on Antarctic first-year sea-ice floes. *Annals of Glaciology* **33**, 51–60. doi: 10.3189/172756401781818266
Jutras M and 7 others (2016) Thermodynamics of slush and snow–ice formation in the Antarctic sea-ice zone. *Deep Sea Research Part II: Topical Studies in Oceanography* **131**, 75–83 doi: 10.1016/j.dsr2.2016.03.008
Knight CA (1988) Formation of slush on floating ice. *Cold Regions Science and Technology* **15**(1), 33–38. doi: 10.1016/0165-232X(88)90035-3
Lei R and 5 others (2014) Multiyear sea ice thermal regimes and oceanic heat flux derived from an ice mass balance buoy in the Arctic Ocean. *Journal of Geophysical Research: Oceans* **119**(1), 537–547. doi: 10.1002/2012JC008731
Lei R and 6 others (2018) Seasonal and interannual variations of sea ice mass balance from the Central Arctic to the Greenland Sea. *Journal of Geophysical Research: Oceans* **123**(4), 2422–2439. doi: 10.1002/2017JC013548
Leppäranta M (1983) A growth model for black ice, snow ice and snow thickness in subarctic basins. *Nordic Hydrology* **14**(2), 59–70. doi: 10.2166/nh.1983.0006
Leppäranta M and Kosloff P (2000) The structure and thickness of lake Pääjärvi ice. *Geophysica* **36**(1–2), 233–248.
Lytle V and Ackley S (2001) Snow-ice growth: a fresh-water flux inhibiting deep convection in the Weddell Sea, Antarctica. *Annals of Glaciology* **33**, 45–50. doi: doi: 10.3189/172756401781818752
Machguth H, Tedstone AJ and Mattea E (2023) Daily variations in Western Greenland slush limits, 2000–2021. *Journal of Glaciology* **69**(273), 191–203. doi: 10.1017/jog.2022.65
Mellor M (1977) Engineering properties of snow. *Journal of Glaciology* **19**(81), 15–66. doi: 10.3189/s002214300002921x
Nicolaus M, Haas C and Bareiss J (2003) Observations of superimposed ice formation at melt-onset on fast ice on Kongsfjorden, Svalbard. *Physics and Chemistry of the Earth* **28**(28–32), 1241–1248. doi: 10.1016/j.pce.2003.08.048
Ohata Y, Toyota T and Shiraiwa T (2016) Lake ice formation processes and thickness evolution at Lake Abashiri, Hokkaido, Japan. *Journal of Glaciology* **62**(233), 563–578. doi: 10.1017/jog.2016.57
Perovich DK (1996) The Optical Properties of Sea Ice. *US Army Corps of Engineers Cold Regions Research & Engineering Laboratory* ((Monograph 96–1).).
Perovich DK, Roesler CS and Pegau WS (1998) Variability in Arctic sea ice optical properties. *Journal of Geophysical Research: Oceans* **103**(C1), 1193–1208. doi: 10.1029/97JC01614
Perovich DK, Tucbker III WB and Ligett KA (2002) Aerial observations of the evolution of ice surface conditions during summer. *Journal of Geophysical Research: Oceans* **107**(C10), SHE-24. doi: 10.1029/2000JC000449
Purdie CR, Langhorne PJ, Leonard GH and Haskell TG (2006) Growth of first-year landfast Antarctic sea ice determined from winter temperature measurements. *Annals of Glaciology* **44**, 170–176. doi: 10.3189/172756406781811853
Ramires ML and 5 others (1995) Standard reference data for the thermal conductivity of water. *Journal of Physical and Chemical Reference Data* **24**(3), 1377–1381. doi: 10.1063/1.555963
Riska K and 8 others (2019) Brash ice growth model – development and validation. *Cold Regions Science and Technology* **157**, 30–41. doi: 10.1016/j.coldregions.2018.09.004
Riska K, Blouquin R, Coche E, Shumovskiy S and Boreysha D (2014) Modelling brash ice growth in ports. *22nd IAHR International Symposium on Ice Singapore*, August 11 to 15, 2014.
Sahlberg J (1988) Modelling the thermal regime of a lake during the winter season. *Cold Regions Science and Technology* **15**(2), 151–159. doi: 10.1016/0165-232X(88)90061-4
Saloranta TM (2000) Modeling the evolution of snow, snow ice, and ice in the Baltic Sea. *Tellus, Series A: Dynamic Meteorology and Oceanography* **52**(1), 93–108. doi: 10.3402/tellusa.v52i1.12255
Sandkvist J (1986) *Brash Ice behaviour in Frequent Ship Channels* (Licentiate dissertation). 139.
Schwerdtfecer P (1963) The thermal properties of sea ice. *Journal of Glaciology* **4**(36), 789–807. doi: 10.3189/S0022143000028379
Sengers JV, Watson JTR, Basu RS, Kamgar-Parsi B and Hendricks RC (1984) Representative equations for the thermal conductivity of water substance. *Journal of physical and chemical reference data* **13**(3), 893–933. doi: 10.1063/1.555718
Shirasawa K and 5 others (2005) The thickness of coastal fast ice in the Sea of Okhotsk. *Cold Regions Science and Technology* **42**(1), 25–40. doi: 10.1016/j.coldregions.2004.11.003
Shirasawa K, Ingram RG and Hudier EJJ (1997) Oceanic heat fluxes under thin sea ice in Saroma-ko Lagoon, Hokkaido, Japan. *Journal of Marine Systems* **11**(1-2), 9–19. doi: 10.1016/S0924-7963(96)00023-1
Shirasawa K, Leppäranta M, Kawamura T, Ishikawa M and Takatsuka T (2006) Measurements and modelling of the water: ice heat flux in natural waters. In *Proceedings of the 18th IAHR International Symposium on Ice*, Vol. 1, pp. 85–91. IAHR.
Stefan J (1889) Uber die theorie der eisbilding, insbesondere uber eisbildung im polarmeere. *Annalen der Physik*, 3rd Serie **42**, 269–286.
Toyota T, Ono T, Tanikawa T, Wongpan P and Nomura D (2020) Solidification effects of snowfall on sea-ice freeze-up: results from an onsite experimental study. *Annals of Glaciology* **61**(83), 299–308. doi: 10.1017/aog.2020.49
Wang C, Cheng B, Wang K, Gerland S and Pavlova O (2015) Modelling snow ice and superimposed ice on landfast sea ice in Kongsfjorden, Svalbard. *Polar Research* **34**(1), 20828. doi: 10.3402/polar.v34.20828
Weeks WF and Lee OS (1958) Observations on the physical properties of sea-ice at Hopedale, Labrador. *Arctic* **11**(3), 134–155.
Yen Y (1981) *Review of thermal properties of snow, ice and sea ice* (CRREL Report 81–10 Review). Hanover, NH: United States Army Corps of Engineers Cold Regions Research and Engineering Laboratory.
Zhaka V, Bonath V, Sand B and Cwirzen A (2020) Physical and mechanical properties of ice from a refrozen ship channel ice in Bay of Bothnia. In *Proceedings of The 25th International Symposium on Ice*. (November), pp. 23–25.
Zhaka V, Bridges R, Riska K and Cwirzen A (2021) A review of level ice and brash ice growth models. *Journal of Glaciology* **68**(270), 685–704. doi: 10.1017/jog.2021.126
Zhaka V, Bridges R, Riska K and Cwirzen A (2022) Slush formation from snow submergence in freshwater. *26th IAHR Inernational Symposium on Ice*, Montréal, Canada, 19–23 June.
Zhaka V, Bridges R, Riska K, Nilimaa J and Cwirzen A (2023) Observations of snow–slush–snow ice transformation and properties of brash Ice in ship channels. *Water* **15**(13), 2360. doi: 10.3390/w15132360

https://doi.org/10.1017/aog.2023.58 Published online by Cambridge University Press